REVIEW ARTICLE

Additive manufacturing of bone scaffolds

Youwen Yang[1,2†], Guoyong Wang[1†], Huixin Liang[3], Chengde Gao[2], Shuping Peng[4], Lida Shen[3] and Cijun Shuai[1,2,5*]

[1]Jiangxi University of Science and Technology, Nanchang 330013, China
[2]State Key Laboratory of High Performance Complex Manufacturing, Central South University, Changsha 410083, China
[3]College of Mechanical and Electrical Engineering, Nanjing University of Aeronautics and Astronautics, 210016 Nanjing, China
[4]Hunan Provincial Tumor Hospital and the Affiliated Tumor Hospital of Xiangya School of Medicine, Central South University, Changsha 410013, China
[5]Key Laboratory of Organ Injury, Aging and Regenerative Medicine of Hunan Province, Changsha 410008, China
†These authors contributed equally to this work.

Abstract: Additive manufacturing (AM) can obtain not only customized external shape but also porous internal structure for scaffolds, both of which are of great importance for repairing large segmental bone defects. The scaffold fabrication process generally involves scaffold design, AM, and post-treatments. Thus, this article firstly reviews the state-of-the-art of scaffold design, including computer-aided design, reverse modeling, topology optimization, and mathematical modeling. In addition, the current characteristics of several typical AM techniques, including selective laser sintering, fused deposition modeling (FDM), and electron beam melting (EBM), especially their advantages and limitations are presented. In particular, selective laser sintering is able to obtain scaffolds with nanoscale grains, due to its high heating rate and a short holding time. However, this character usually results in insufficient densification. FDM can fabricate scaffolds with a relative high accuracy of pore structure but with a relative low mechanical strength. EBM with a high beam-material coupling efficiency can process high melting point metals, but it exhibits a low-resolution and poor surface quality. Furthermore, the common post-treatments, with main focus on heat and surface treatments, which are applied to improve the comprehensive performance are also discussed. Finally, this review also discusses the future directions for AM scaffolds for bone tissue engineering.

Keywords: Additive manufacturing; bone scaffolds; scaffolds design; post-treatments

*Correspondence to: Cijun Shuai, Central South University, China; shuai@csu.edu.cn

Received: June 09, 2018; **Accepted:** July 09, 2018; **Published Online:** December 12, 2018

Citation: Yang Y, Wang G, Liang H, *et al*., 2019, Additive manufacturing of bone scaffolds. *Int J Bioprint*, 5(1): 148. http://dx/doi.org/10.18063/IJB.v5i1.148

1. Introduction

Bone tissue is able to subject to biological remodeling through a dynamic process of the absorption of mature bone tissue by osteoclasts and subsequent generation of new bone induced by osteoblasts[1,2]. Nevertheless, the body usually cannot fulfill the self-repairing as a large segmental bone defect occurs, in which the bone defect exceeds a critical size of about 10 mm[3]. In this condition, an external intervention is required to aid in the self-repairing by means of building bridges on the bone defect site[4]. Therefore, bone grafts are extensively required in clinical surgeries to aid in the healing of these large segmental bone defects. Data from the center for disease control show that bone is the second most commonly graft tissue, with more than 2 million surgical operations utilizing bone grafts annually[5]. Autografts taken from the patient-self are considered as the gold standard for bone repair[6]. However, the size of the autograft is very limited. Moreover, harvesting the autograft inevitably causes an additional surgical trauma associated with a serious risk of morbidity at the donor site. Allografts taken from other persons are an alternative and are in larger supply as compared with the autografts. However, they usually lead

to disease transmission and immune rejection[7]. Thus, idea bone substitutes are urgently demanded for bone tissue repair in surgical application.

Desired bone substitutes should have a customized external shape, aiming to avoid the excess removal of bone tissue at defect sites. More importantly, they also need to have porous and interconnected pore structure, so as to create a microenvironment, which is conducive to cell activity and reproduction[8,9]. To obtain scaffolds with the porous structure for bone repair, several approaches, such as pore-forming agent method[10,11], gas foaming method[12,13], sol-gel method[14,15], and freezing drying method[16,17], have been proposed. Although these methods exhibit a certain ability to fabricate porous structure, they are also with some limitations, such as inaccurate control of the pore structure and poor ability to customize for specific defect sites[18]. Moreover, some of these approaches inevitably leave some organic residues of pore-forming agent, which will reduce the biological properties of the scaffolds and sacrifice the quality of bone repair. Therefore, exploring a fabrication technique that is not only limited to obtain the individual external shape but also accurately control the pore structure for scaffolds is of great significance for their further orthopedic application.

Additive manufacturing (AM) can produce a porous scaffold with individual external shape and porous internal structure[19]. Before AM process, a three-dimensional (3D) scaffold model is generally designed with desired architecture using computer-aided design (CAD) software. The 3D scaffold model is sliced into a series of two-dimensional (2D) slices before converting to typical Stereolithography (STL) files, which contain detailed 2D slice information. Based on these STL files, an AM machine performs the necessary toolpath along the 2D directions for direct building of 2D layers. Each layer is just built on top of the other to construct a 3D part. Due to the fabrication process of adding one layer on the previous one, this manufacturing technique is described as AM. Currently, researchers around the world are committed to apply AM techniques to produce porous implants for bone repair. For instance, Poukens[20] successfully applied AM to fabricate porous mandible implant, which was subsequently implanted in a patient. Brazilian Jardini *et al*.[21] used an AM processed customized porous scaffold to repair a large cranial defect. Australian Peter[22] implanted the AM-derived porous titanium implants into a 71-year-old patient who faced an amputation of the heel bone. All these successes positively render the AM techniques a promising future for bone tissue repair.

A typical application of porous scaffolds fabricated by AM includes the scaffolds design, AM, and post-treatments, as schematically illustrated in Figure 1. Therefore, this work reviews the overall process for AM of bone

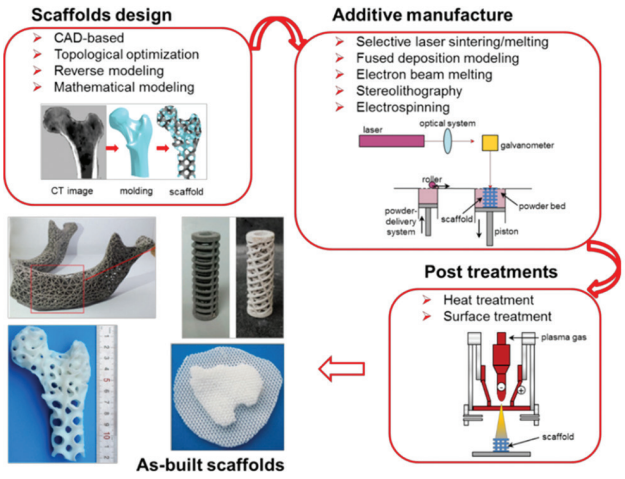

Figure 1. A schematic diagram for the design, additive manufacturing (AM), post-treatments of bone scaffolds, and several typical AM-derived scaffolds. Images adapted from references[29-32].

scaffolds. Several typical structure design methods are first examined, especially the mathematical modeling method, which can achieve with both bionic design and topological optimization of scaffolds. Following on, the most relevant AM techniques using for scaffolds fabrication, with their advantages and disadvantages, are highlighted. The common post-treatments related to AM-derived scaffolds are also discussed. Finally, the future trends for AM scaffolds for bone repair are addressed.

2. Scaffold Design

Scaffold design is an important step in AM bone scaffolds. This is because the features of the porous structure, including the porosity, pore size, and pore interconnectivity, have great influence on their biological performance and mechanical properties[23-25]. In particular, an appropriate pore size and high porosity facilitate the absorption of nutrients and the excretion of metabolic waste, thus providing a suitable environment for the growth of bone tissue[26]. Meanwhile, the internal pore structure and the distribution of materials directly influence the plasticity and stiffness, thus determining the stress environment of the surrounding bone tissue as implanted *in vivo*[27]. Besides, the mechanical function of the scaffolds dynamically changes after implantation, which should be taken into consideration in scaffolds design. On the other hand, the external shape features of the scaffolds should conform to the morphological characteristics of the defect site to obtain the desired shape. It should be noted that the designed scaffolds are required to easily build using specific AM techniques. For instance, the overhanging structure commonly causes some undesirable defects, if a corresponding supporting structure is absent when it is building[28].

2.1. CAD-Based Method

CAD-based method, the most common method for scaffolds design, is realized by utilizing various CAD tools, such as UG, CATIA, and Pro/E.[33,34]. These CAD tools construct models based on constructive solid geometry (CSG) or boundary representation (B-Rep) principle. In the CSG method, specific models are constructed using a series of Boolean operations with standard solid primitives, such as the cubic, cylinder, ball, and prism, whereas, in B-Rep method, the solid models are depicted using their boundaries. The typical boundaries include vertices, edges, and loops, with no direct relation among them[35]. Models obtained by B-Rep require more storage space, as compared to CSG. Therefore, as the model becomes larger or has a more detailed internal structure, the size of the file containing B-Rep-derived model will increase dramatically, causing great difficulty in further operation.

Based on the above-mentioned modeling principles, CAD tools construct various porous unit cells and assemble them to build the whole scaffolds. A series of unit cells have been designed to characterize the architecture of bone scaffolds[36,37]. Melchels *et al.*[38] designed three sophisticated unit cells, including a cube, a diamond, and a gyroid. While space-filling computer models with distinct architectures were generated from assemblies of these unit cells, as shown in Figure 2A. Finite element simulations of the compression behavior indicated that gyroid architecture presented more homogeneous distribution of stress and strain, as compared to cube architecture (Figure 2B). Thus, scaffolds with gyroid architecture are believed to expose adherent cells with relatively more equal mechanical stimuli, which might be more beneficial for bone regeneration. Sercombe *et al.*[39] designed a unit cell with octahedral geometry. Finite element analysis of the failure mechanisms revealed that this structure could bear high tensile stress.

To simplify the CAD-based design process, some dedicated design software has been successfully developed. For instance, Belgium Materialise Company has developed a 3D printing pre-processing software named Magics, in which designers can directly instruct various integrated unit cells. Murr *et al.*[40] reported a case of quickly building scaffolds using MATERAILAS software elements, including cross 1, G6, G7, and code thin, as shown in Figure 2C. Researchers also developed a computer-aided system for tissue scaffolds (CASTS), which included a parametric library of scaffold structures and an algorithm to define the pore size, porosity, and surface-to-volume ratio[33,41]. With CASTS, designers can obtain desired scaffold models with proper porosity and pore size by setting a series of parameters. Although CAD-based design shows powerful design ability, it

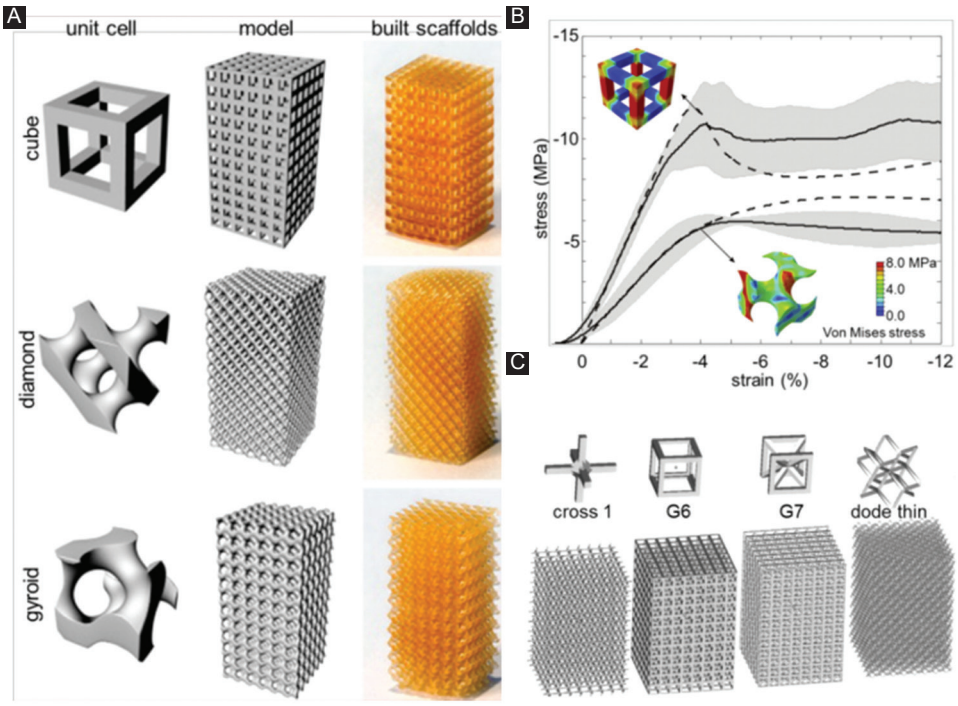

Figure 2. (**A**) Computer-aided design-based unit cells with cube, diamond, and gyroid architecture, as well as their assemblies and as-built scaffolds. (**B**) Stress-strain curves of the scaffolds with cube and gyroid architecture[38]. The obtained data are described as the averages in solid lines with standard deviation in shaded areas, and finite element results are depicted in dashed lines. (**C**) Materialise Software elements and designed scaffold models[40].

exhibits poor controllability on the structural performance and mechanical properties of designed scaffolds. Moreover, there is an ineffaceable staircase phenomenon on the external contour of models caused by Boolean operation, leading to geometric distortion and mechanical instability[42]. Besides, the CAD-based method can only design the scaffolds with periodic and regular structure.

2.2. Topology Optimization

Ideal bone scaffolds should not only have highly porous structure to facilitate cell in-growth and nutrient transport but should also possess enough mechanical properties to provide stable structure support[30,43-45]. Paradoxically, increasing the porosity of the scaffolds enhances the material transport capacity but inevitably impairs the mechanical properties. Thus, the scaffold designer should balance these two conflicting properties to obtain an optimal comprehensive performance. Topology optimization is a method to optimize the distribution of materials in a given region based on the given load condition, constraint condition, and performance index[46]. Designing scaffolds with topology optimization is expected to achieve an optimized comprehensive performance with certain constraints, for example, the maximum mechanical properties with certain porosity or maximum permeability. In topology optimization of scaffolds, the optimization problem is generally solved indirectly through optimizing a unit cell with specific optimization algorithms. After obtaining the optimized unit cell architecture, the whole scaffold is formed by repeating it periodically. The classic optimization algorithms applied in topology optimization of scaffolds include Solid Isotropic Material with Penalization (SIMP) method and evolutionary structural optimization (ESO) method, which describe the structure point-by-point in topology optimization[47]. Guest *et al.* [48] optimized a scaffold based on the SIMP optimization algorithm, in which two competing properties, including the modulus and permeability, were tailored using a single objective function[49]. SIMP method is also applied to optimize the elastic tensor of scaffolds[50]. *In vivo* tests showed that the optimized scaffolds with similar elastic properties to that of human bone exhibited an accelerated bone remodeling rate. Besides, a series of unit cells with maximal shear and bulk modulus, predefined stiffness ratios and functionally graded structure, were obtained through the ESO-based topology optimization[51]. Some scaffolds optimized by bidirectional evolutionary ESO method, which obtain the maximum bulk or shear modulus under various prescribed volume fractions, are depicted in Figure 3[52].

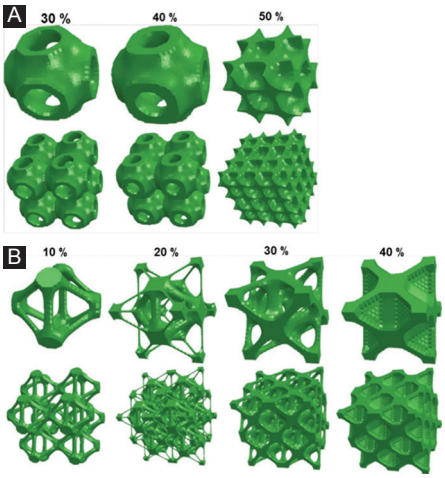

Figure 3. Topology optimized unit cells and scaffolds with (**A**) maximum bulk modulus and (**B**) maximum shear modulus under various predefined volume fractions[52].

Another typical topology optimization method is level-s*et al.*orithm, which centers on tracing the phase boundaries, thus effectively describing smooth boundaries to control the topology changes[53]. A level-set based method for scaffolds design was proposed to obtain material with maximal permeability[54]. Level-set based topology optimization made it possible that the no-slip boundary condition of fluids in Stokes flow could be naturally satisfied[55]. Topology optimization was also reported to tailor the thermal expansion of porous multimaterials[56]. However, as mentioned before, the topology optimization of the scaffolds begins with the optimization of the unit cells and proceeds with the subsequent periodic arrangement. Therefore, it can only achieve regular porous architecture, which is considerably different from the irregular structure of natural bone.

2.3. Reverse Modeling

Reverse modeling design, also known as image-based design, reconstructs bone tissue microstructure directly based on object's computed tomography (CT) or magnetic resonance imaging (MRI)[57]. In this method, the CT/MRI slice images undergo a series of analysis, with an aim to extract the key features for reconstruction. Binary value method is commonly used to analyze the slice information, in which element "1" represents the solid, whereas "0" represents the void[58]. Then, the pre-defined unit cell is mapped according to the extracted slice information to construct the 2D model. This 2D model will directly be transformed into STL files and transmitted to an AM equipment to construct 2D layer. After this, a 3D part is obtained using the layer-by-layer method. Obviously, reverse modeling design combines advanced medical imaging system, powerful image analysis software as well as rapid AM technique, which guarantees a more mimic architecture for bone tissue engineering.

Reverse modeling has appealed to a large number of researchers for constructing customized scaffolds. Sun *et al.* [59] systematically investigated the modeling principles and

the unit library approach to biomimetically create porous structures. Similar method approach was also researched by Hollister *et al.*[60,61] by creating the internal architecture by altering the density in the voxel dataset. Based on these early studies, Podshivalov *et al.*[62] constructed microscale structure scaffolds based on the processing of actual micro-CT images followed by reconstructing a highly accurate geometrical model, which resembles the actual trabecular bone structure. Related studies showed that the porous structure obtained by reverse modeling was more conducive to the growth of cells, which also proved the superiority of irregular porous structure[63,64].

Although reverse modeling design can obtain the porous structure that perfectly coincides with the natural bone, the accuracy of the model highly depends on the resolution of the image acquisition device. On top of that, it needs a lot of computing resources and storage space and proposes higher requirements for software developers and users.

2.4. Mathematical Modeling

Mathematical modeling mainly utilizes shape functions to construct porous scaffolds with implicit function surfaces or irregular polygonal models, which breaks through the geometry limitations of the traditional porous element. Among them, triply periodic minimal surface (TPMS) method uses trigonometric functions to derive a complex porous structure with a minimal surface, in which the curvature at any point is zero[58]. The TPMS structure also presents a periodicity in three independent directions due to the periodic characteristic of the trigonometric function, with no sealed cavities exist in the geometry[65]. In fact, the examples of the minimal surface geometry exist in nature, including beetle shells, butterfly wings, and crustacean bones[66].

Rajagopalan *et al.* first proposed a TPMS-based method for designing tissue scaffolds and a simple primitive (P-type) unit[67]. Other types of TPMS units including diamond (D type) and gyroid (G type) were also proposed for bone scaffolds design[68], as shown in Figure 4A. Studies on the influence of these morphologies on cell migration revealed that the scaffolds with

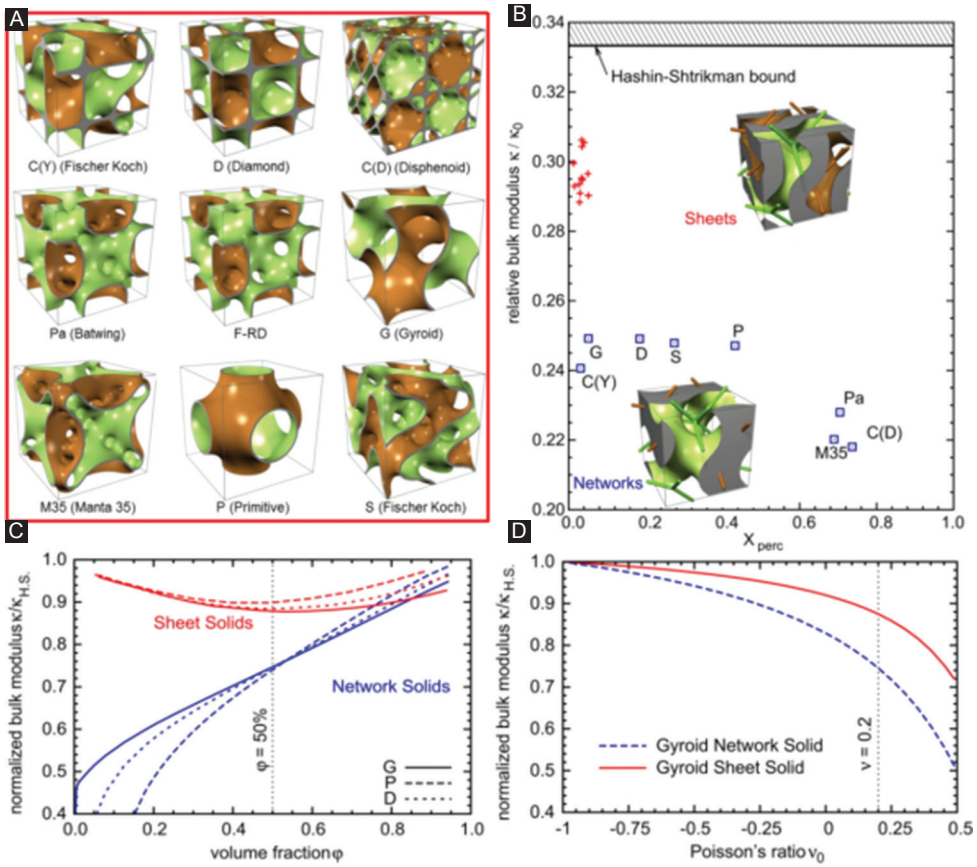

Figure 4. (**A**) Various triply periodic minimal surface (TPMS) unit cells for bone scaffolds design[68]. (**B**) The relative bulk modulus of TPMS scaffolds with a volume fraction of 50% and Poisson's ratio 0.2. The blue boxes indicate the network solids, whereas the red crosses indicate the sheet solids. X_{perc} represents the dimensionless non-percolation ratio. Insets are two kinds of scaffold structure based on the gyroid-type TPMS with the volume fraction of 50%. The curves showed the relationships between the stiffness and volume fraction (**C**) and Poisson's ratio (**D**). With identical volume fraction or Poisson's ratio, sheet solid scaffolds exhibited higher stiffness as compared with network solid scaffolds.

minimal surfaces were more easily wetted with higher permeability, leading to deeper cells into growth as well as more uniform cell distribution, as compared with a salt-leached scaffold with a random-pore architecture[69]. Kapfer *et al.*[68] investigated two kinds of TPMS-based structure, including network solids and sheet solids. In the network solids, the minimal surface constructs the solid/void interface, whereas in sheet solids, porous solids are constructed by inflating the minimal surfaces to sheets with a predefined thickness. Finite element analysis confirmed that the sheet solids possessed considerably higher mechanical stiffness than that of network solids for identical volume fractions (Figure 4B and C) and Poisson's ratio (Figure 4D). Moreover, the sheet solids also exhibited higher material utilization and provided relatively more surface area and pore space for cell migration and activity.

TPMS has been explored for its possibility to construct gradient, heterogeneous, hybrid, and irregular porous structures. Melchels *et al.*[38] reported that the design of a gradient porous structure can be constructed based on TPMS by adding a linear function. Feng *et al.*[31] designed heterogeneous porous scaffolds with non-uniform threshold, period, and unit by combining TPMS and solid T-splines. In addition, Yang *et al.*[70] proposed two CAD methods to prepare hybrid porous structures for biomimetic design purposes that combine different TPMS-based structures with given transition boundaries. Using his approach, it is able to place TPMS-based substructures on given 3D subspaces with perfect transitions to their adjacent substructures within a scaffold domain. A series of multiscale and multimorphology porous scaffolds were presented in their further studies[71-74]. For similar goals, Yoo *et al.*[75-77] combined a kind of distance field with TPMS-based functions to effectively construct pseudorandom porous scaffolds. Yang *et al.*[78] utilized coordinate transformation based on TPMS to construct an gradient and full irregular porous structure, extending TPMS to irregular design areas. However, the stochastic porous structure constructed by this method had porosities lower than 74%. Beyond this critical point, the solid phase turned disconnected.

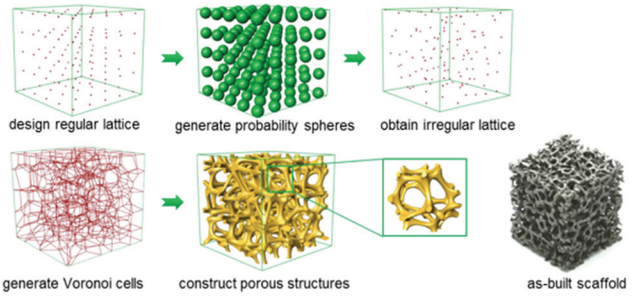

Figure 5. A schematic diagram showing the scaffold design principle based on Voronoi-Tessellation method and as-built scaffolds[87].

Another typical mathematical modeling is Voronoi-Tessellation method, which constructs porous models using a Voronoi diagram. A typical scaffold design principle based on Voronoi-Tessellation method is depicted in Figure 5. In particular, a set of points (or seeds) are positioned randomly inside the design volume to fulfill a partition of the space in regions. Then, a thickness is assigned to the edges of the partitioned regions to obtain a porous scaffold[79,80]. The design of porous structure based on Voronoi diagram could be traced back to Kou and Tan[81,82], where they first proposed to use Voronoi vertices as the control points of a closed B-spline curve to create a convex-shaped cell. Besides, a porous structure was obtained by merging the adjacent cells. However, they only studied the 2D pore structure. While Chow *et al.*[83] organized Voronoi seeds in concentric circles and formed a 2D shape region. Subsequently, a 3D porous structure was constructed by expanding the time dimension of the dynamic pattern in the third dimension of the 2D shape region.

In recent years, researchers have conducted a more in-depth study on Voronoi-Tessellation-based scaffold design and have achieved great progress. For example, Fantini *et al.*[84] combined CAD 3D software Rhinoceros with its Plug-in Grasshopper to design bone scaffolds based on Voronoi-Tessellation method. This work successfully correlated to the input parameters, including the number of seeds, porosity, and the pore size of the structure[85]. Gómez *et al.*[86] proposed a bone-like trabecular structure design based on Voronoi-Tessellation principle. The seeds of Voronoi diagram were extracted from the micro-CT images of the trabecular bone. The obtained isotropic porous scaffolds were then perfectly matched the main histomorphometric indices of nature bone. More importantly, the final properties could be tailored during the design stage by changing the trabecular separation and thickness. Wang *et al.*[87] put forward a probability sphere method to generate random seeds based on the Voronoi-Tessellation. In this study, a scale coefficient K was introduced to control the pore size and strut thickness, which successfully achieved the balance between "irregularity" and "controllability." As a result, highly mimic scaffolds with porosities ranging from 60% to 95% and pore size ranging from 200 to 1200 μm were designed precisely. In addition, a porosity gradient ranging from 0.03 to 0.54 was also obtained. In this regard, it is clear that Voronoi-Tessellation method combines the advantages of reverse modeling method and topology optimization method. It cannot only realize the bionic structure design of bone scaffold but also optimize the structure to achieve desirable properties, such as porosity, permeability, and mechanical strength.

Nevertheless, further investigations using *in vitro* and *in vivo* studies are needed to confirm their biological properties.

3. AM of Bone Scaffolds

The AM technique, which emerged in the 1980s, can rapidly produce scaffolds with external complex contour and internal porous structure. Combining with CT data obtained from the injury sites, AM can produce customized implants in a very short period, thus showing great prospects in orthopedic application. Up to now, many AM techniques exhibit their powerful ability to fabricate complex bone implants. This includes well-developed methods, such as selective laser sintering (SLS), selective laser melting (SLM), fused deposition modeling (FDM), electron beam melting (EBM), stereolithography (SLA), and electrospinning. Meanwhile, the developing AM techniques, including continuous liquid interface polymerization[88] and two-photon polymerization[89], also demonstrate great potential for scaffold fabrication. In this chapter, we only focus on the several most relevant AM techniques for the fabrication of bone scaffolds. Scaffold-based AM method can process a wide range of biomaterials, including metals, polymer, and ceramics. On top of that, the prepared scaffold can provide appropriate biomechanical and biochemical conditions for cell proliferation and ultimate tissue formation. In comparison, scaffold-free AM method mainly utilizes multicellular bio-ink to construct 3D tissue and organ, which focuses on preparing soft tissue[90,91].

3.1. SLS

The principle of SLS was first proposed in 1986[92]. In brief, an SLS system mainly consists of a laser, powder bed, a piston to move down in the vertical direction, and a roller to spread a new powder layer. The computer-controlled laser beam sinters the powder, while the untreated powder serves as a structural support for the

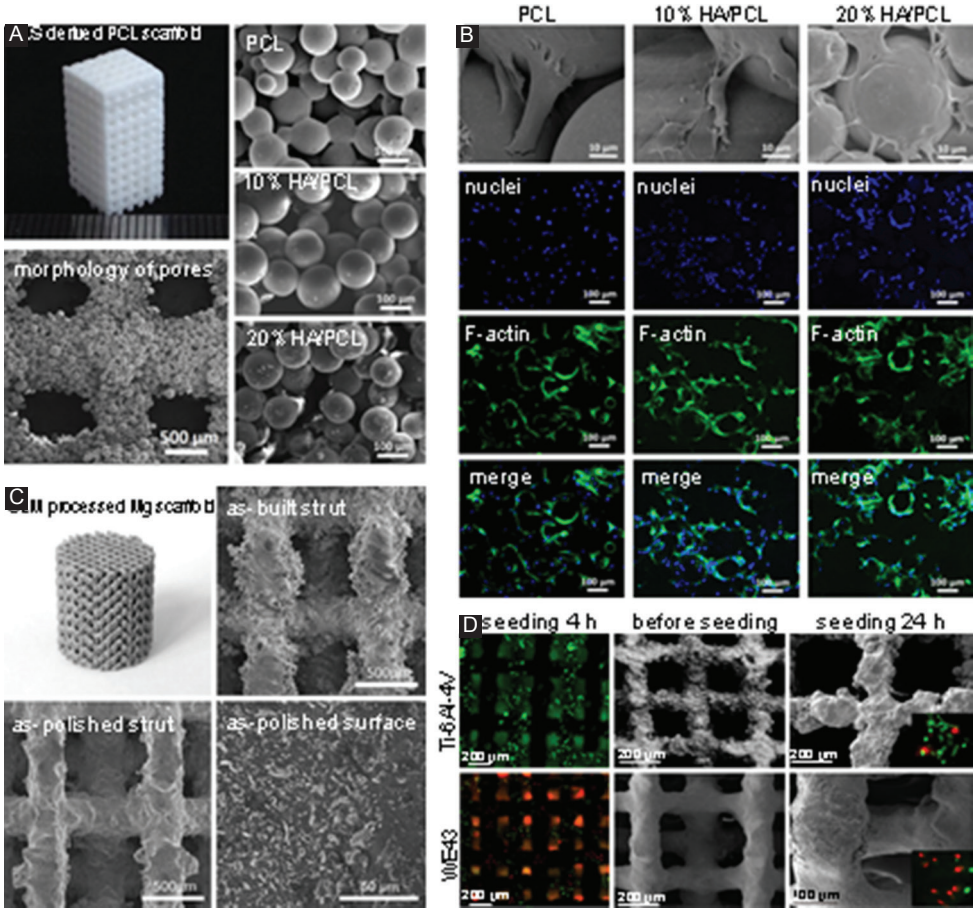

Figure 6. (**A**) Selective laser sintering (SLS)-derived poly(ε-caprolactone) scaffold, with scanning electron microscope (SEM) images showing the morphology of pores and well-connected microspheres[99]. (**B**) *In vitro* evaluation of SLS-derived scaffolds, with SEM and confocal images showing the morphologies of adherent mesenchymal stem cells on the scaffolds after culturing for 12 h. (**C**) Selective laser melting (SLM) processed Mg-based scaffold (WE43), with SEM images showing the surface morphology and microstructure[124]. (**D**) *In vitro* evaluation of SLM-derived WE43 and Ti-6Al-4V scaffolds. Fluorescent optical images showed the morphologies of MG 63 cells on scaffolds, in which live cells were stained in green, whereas dead cells were stained in red.

scaffold being built.

SLS usually refers to solid or semisolid consolidation mechanisms at a sintering temperature lower than melting point[93]. In semisolid sintering, powder particles are partially melted and form a small amount of liquid phase, which bonds other solid particles to become solid parts. SLS with semisolid consolidation mechanisms is suitable for processing low melting point polymer, such as polylactic acid (PLA)[94], polyglycolide[95], poly(L-lactide) (PLLA)[96], and poly(ε-caprolactone) (PCL)[97]. Researchers also used SLS to process the polymer and ceramic composites. Du *et al.* reported that a microsphere-based hydroxyapatite (HA)/PCL composite scaffolds constructed by SLS[98,99], which shows a highly ordered porous structure, as shown in Figure 6A. Scanning electron microscope (SEM) images confirmed that the microspheres were well connected through laser sintering in the composite scaffolds. *In vitro* assays showed that the scaffolds promoted cell adhesion, cell proliferation, as well as cell differentiation (Figure 6B). In addition, *in vivo* assay demonstrated an excellent histocompatibility and promotion of new vascularization tissue. Kumaresan *et al*.[100] successfully applied SLS to fabricate polyamide/HA composite scaffolds with porosities ranging from 40% to 70%. With an optimal HA content of 15 wt.%, optimal mechanical properties with a maximum tensile strength of 21.4 MPa and a compression stress of 25.2 MPa were obtained.

SLS can also process bioceramic scaffolds, such as HA[101], β-tricalcium phosphate (β-TCP)[102], and bioglass[103]. It is well known that bioceramics commonly have higher melting point as compared to polymers. Thus, SLS of bioceramic is generally based on the solid consolidation mechanism[104]. Specifically, high-energy laser beam acts on the ceramic particles, increases the surface temperature, and promotes the particles approach to each other before sintering together. Meanwhile, the material on the grain boundary continues to diffuse to the pores, which promotes the densification behaviors. Nevertheless, SLS has a very short sintering period, due to its high heating rate and short holding time[105]. Such a short sintering period can effectively restrain the diffuse of grain boundaries, which enables SLS to obtain ceramic scaffolds with nanoscale grains. Moreover, SLS exhibits great potential in fabricating scaffolds reinforced by low-dimensional nanomaterials (LDNs), such as carbon nanotubes, graphene, and boron nitride nanotubes[106]. This is because the short sintering period combined with low sintering temperature can avoid destructing the structure of LDNs[107]. Mechanical tests and *in vitro* cell culture confirmed their enhanced mechanical properties and improved biological properties, respectively[105,108].

Special care should be taken with regard to the limited liquid formation in SLS, which causes insufficient densification and heterogeneous microstructures. To solve this problem, an introduction of low melting point infiltration into SLS is an alternative method to promote the liquid phase formation and the crystallite rearrangement, thus enhancing the densification behavior. Duan *et al*.[109] introduced CaO-Al_2O_3-SiO_2 as a liquid phase into HA scaffolds in SLS. The improved densification in sintering led to enhanced mechanical properties, with the compression strength, fracture toughness, and hardness increased by 105%, 63%, and 11%, respectively. Liu *et al*.[110] also reported an increase of 18.18% in fracture toughness after introducing PLLA as a liquid phase into β-TCP scaffolds.

3.2. SLM

SLM is initially designed for 3D freeform fabrication of metals[104]. Compared with SLS, SLM applied higher energy density laser to fulfill a complete melting/solidification mechanism[111]. Thus, SLM-derived parts normally have an improved surface quality, density, and resultant superior mechanical strength. In consideration of the high-energy density, SLM is mainly applied to process metal scaffolds. Čapek *et al*.[112] prepared a highly porous (87 vol.%) 316 L stainless steel scaffold as joint replacement by SLM. The scaffolds exhibited similar mechanical properties to those of trabecular bone with a compressive modulus of elasticity 0.15 GPa and compressive yield strength of 3 MPa. Weißmann *et al*.[113] reported that Ti-6Al-4V porous scaffolds are formed with 3.4 and 26.3 GPa and porosity ranging from 54% to 60%. Besides, it also revealed a clear influence of the unit cell orientation on elastic modulus, compressive strength, and strain. Wang *et al*.[114] evaluated the effects of parametrical variations on the mechanical properties of SLM-derived scaffolds. Results revealed that porous design could reduce the effective modulus of scaffolds by 75–80%. Shah *et al*.[115] used SLM to produce Ti-6Al-4V scaffolds for load-bearing orthopedic applications. The bone/scaffold interface was studied after implantation in an adult sheep for 6 months. The compressive strength ranged from 35 to 120 MPa as the porosity ranged from 55% to 75%.

Recently, biodegradable metals, mainly Mg and Zn alloys, have drawn an increasing interest of researchers, due to their inherent degradability as well as close mechanical properties to that of natural bone[116-119]. At present, the main problem of Mg alloys as bone implants is their poor corrosion resistance. Surprisingly, recent studies revealed that SLM-processed Mg alloys exhibited improved corrosion resistance. This could be ascribed to that SLM involved a rapid solidification, resulting in grains refinement and reduced composition segregation, both of which made contribution to the enhanced corrosion resistance of biodegradable Mg alloys[4,120-122]. However, SLM of Mg alloys is still technically challenging. This is because Mg possesses a very active chemical property and is flammable even at

bulk state. In addition, the melting point of Mg is very close to the boiling point. In spite of those, our research group explored the application of SLM to prepare porous Mg with a home-made SLM system[123]. Under the protection of Ar gas, an Mg scaffold was successfully formed at optimized process parameters. Li *et al.*[124] also successfully prepared porous Mg alloy (WE43) scaffolds by SLM, as shown in Figure 6C. Mechanical tests revealed that the obtained Mg scaffolds exhibited sufficient Young's modulus of 700–800 MPa, which was comparable to trabecular bone after biodegradation for 4 weeks. The Mg scaffolds showed a proper degradation rate (20% volume loss after immersion for 4 weeks) and good compatibility (level 0 cytotoxicity) (Figure 6D). As for Zn and its alloys, the low melting and boiling points also challenge their process stability in SLM. SLM of Zn powder easily causes a large amount of plume due to the metallic vapor. The formed plume will change the optical properties of the laser beam, such as the beam profile and the energy density. These reduce the process stability and cause poor part quality. To address these issues, Grasso *et al.*[125] applied an *in situ* monitoring approach to detect the unstable process behaviors and anticipated severe defects in SLM of pure Zn. Besides, some researchers explored the use of SLM to prepare bulk Zn for bone tissue repair[126-128]. However, to our best knowledge, there are few reports regarding SLM of Zn alloys scaffolds. Instead, a technique merging both gravity casting and 3D printing achieved success in producing porous Zn scaffolds[129].

3.3. FDM

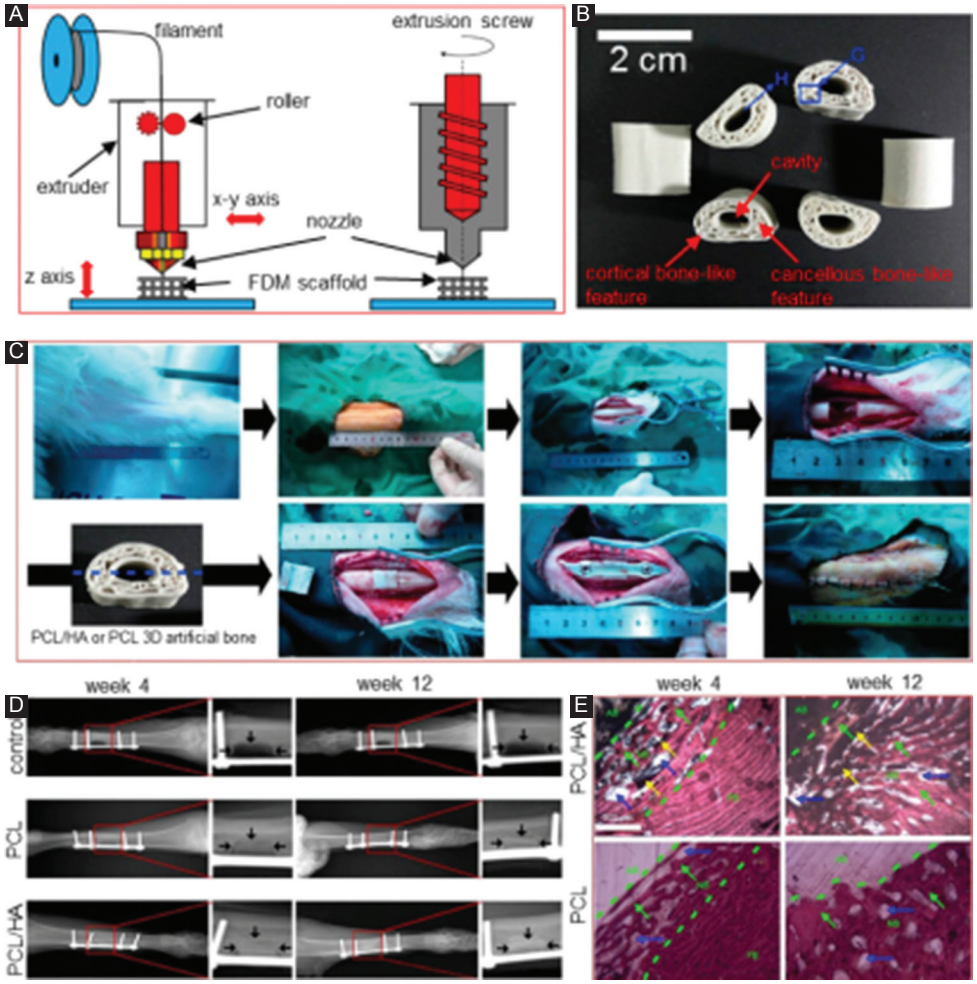

Figure 7. (**A**) A diagram for fused deposition modeling (FDM) process. (**B**) The FDM-derived poly(ε-caprolactone)/hydroxyapatite (PCL/HA) scaffolds[139]. (**C**) The implantation of FDM-derived PCL/HA scaffolds. (**D**) X-ray images of the goat legs after implantation for 4 and 12 weeks, in which the arrows mark the bone defect edges. (**E**) Histological imagines showing the interfaces between the scaffolds and the surrounding tissue. AB represents artificial bone, FB represents natural goat femur bone, and NB represents new bone. The scaffolds were filled with new bone after 12 weeks' implantation.

FDM, also known as extrusion-based processes, was first put forward by Crump in 1988. In FDM, the materials are heated up until flowing before extruding or squeezing out of a nozzle. The extruded fluid subsequently deposited on the substrate with a layer-wise pattern based on the motion of the nozzle in each layer; then, a 3D scaffold is built layer by layer. A diagram for the FDM process is depicted in Figure 7A. The accuracy of extruded scaffolds greatly depends on the printing nozzle.

FDM technology is mainly applied to process low-fusing temperature polymer. Hutmacher *et al.*[130] reported a use of FDM to fabricate porous scaffolds with PCL, which presented 0°/60°/120° orientation patterns with the porosity more than 56% and pore sizes ranging from 380 to 590 μm. Zhou *et al.*[131] fabricated hierarchical polymer scaffolds with macropores between 100 and 800 μm through the FDM. It was demonstrated that porosity printing errors between the obtained scaffolds and the designed model were <5%, indicating that FDM is an efficient technology to obtain scaffolds with a relative high accuracy of pore structure. Tellis *et al.*[132] combined micro-CT and FDM to produce polybutylene terephthalate scaffolds before applying for trabecular repair. Kosorn *et al.*[133] reported that PCL/poly(hydroxybutyrate-co-valerate) (PHBV) blended porous scaffolds fabricated by FDM, founding that the compressive strength increased with incorporated PHBV increasing. Composite scaffolds based on PCL and poly(ethylene glycol) (PEG) were also fabricated by FDM[134].

Recently, polymers with a relative high melting point have also been utilized in FDM. For example, polyether ether ketone (PEEK) with superior melting point between 330°C and 340°C was developed into scaffolds with a self-developed FDM system[135]. In this system, the syringe consists of two different metal tubes, including a brass tube with an internal diameter of 17 mm attached to a 500 μm nozzle and a stainless steel tube. The brass tube with a good thermal conductivity was able to help PEEK absorbed sufficient energy to get fully melted. Controlling the nozzle temperature between 400°C and 430°C and the extrusion rate of 2.2 mg/s, PEEK scaffolds with 38% porosity were successfully obtained, which showed a compressive yield strength of 29.34 MPa and a compressive yield strain of 4.4%. Furthermore, Rinaldi *et al.*[136] also reported a potential usage of FDM in fabricating PEEK scaffolds. However, with high melting point polymers in FDM, severe shrinkage, warpage, and delamination normally occur due to the sharp temperature gradient caused by the relative high extrusion temperature. Therefore, it is necessary to control the cooling process in FDM.

FDM has also been reported for the preparation of polymer and ceramic composite scaffolds[137,138]. Xu *et al.*[139] used CT-guided FDM to fabricate PCL/HA bones scaffolds with cortical bonelike features, as shown in Figure 7B. The scaffolds exhibited close mechanics to that of natural bone in regard to structure feature and chemical composition. *In vivo* assays confirmed their enchanted biodegradability and improved new bone formability (Figure 7C, 7D and 7E), as compared to pure PCL scaffolds. Besides, Kim *et al.*[140] produced a scaffold composed of polylactic-co-glycolic acid (PLGA) and β-TCP by FDM. After 12 weeks' implantation, the scaffolds integrated tightly with the surrounding bone tissue, indicating their good biocompatibility. Poh *et al.*[141] fabricated composite scaffolds containing PCL and bioglass by FDM. Interestingly, *in vitro* tests revealed that the composite scaffold showed an upregulation of osteogenic gene expression. In addition, it was found that the host tissue infiltrated well into the scaffolds after 8 weeks' implantation into the nude rats. Though introducing bioactive ceramics can improve the biological properties of polymer scaffolds but also brings other concerns. During FDM of composites, the incorporated bioceramics with higher melting point exist in solid phase, which will increase the viscosity and reduce the fluidity of the slurry and ultimately reduce the accuracy and efficiency of the molding. On the other hand, due to the different shrinkage characteristics, a large number of pores will form between the ceramic particles and matrix, which greatly reduces its mechanical properties. Therefore, a further process is required to compensate for mechanical properties loss.

3.4. EBM

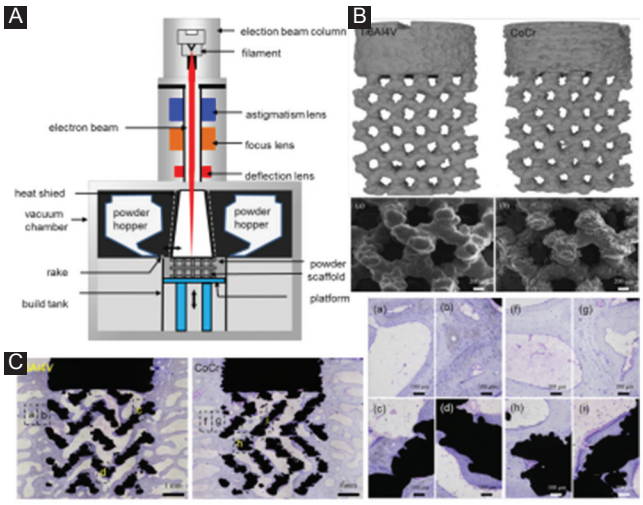

Figure 8. (**A**) A schematic diagram for electron beam melting (EBM) equipment. (**B**) Micro-computed tomography images showing the geometry of EBM-processed scaffolds, and scanning electron microscope images showing the responding roughness surface[147]. (**C**) Undecalcified toluidine blue stained images showing the pattern of bone formation after the implantation of EBM-derived Ti6Al4V and CoCr scaffolds.

EBM was first developed and patented by Swedish Arcam Company[142]. The EBM equipment is mainly composed of an electron beam gun compartment and a specimen-fabrication compartment, both of which are kept in a high vacuum (Figure 8A). Unlike SLS or SLM, EBM technology applies high-energy electron beam to melt the metal powder. The electron beam commonly scans the powder layer quickly before EBM, with an aim to preheat the powder bed and reach to a slight-sintering state. Following on, the electron beam selectively scans the powder layer based on 3D hierarchical data, enabling the preheated powder to melt and solidify together.

Compared to SLS/SLM, a primary advantage of EBM is that it has high beam-material coupling efficiency, which makes it easily process metals with an extreme high melting point[143]. Thus, extensive researches are focused on utilizing EBM to produce porous metal scaffolds. Yan *et al.*[29] reported a case that a 3D Ti scaffold was designed based on a volunteer with whole mandible defect and fabricated through EBM. After implantation, the grafted mandibular recovered well, showing a great potential of EBM in the bone graft. Ataee *et al.* produced Ti-6Al-4V gyroid scaffolds by EBM, which exhibited extreme high porosities ranging from 82% to 85%. In addition, the obtained yield strength and elastic modulus were in the range of 13.1–15.0 MPa and 637–-1084 MPa, respectively, which were comparable to those of trabecular bone[144]. Surmeneva *et al.*[145] fabricated triple- and double-layered Ti-based scaffolds by EBM. Mechanical tests revealed that these scaffolds with gradient porosities of 21–65% had a compressive strength of 31–212 MPa and elastic modulus of 0.9–3.6 GPa, respectively. The compressive strength, elastic modulus, and deformation behavior of EBM-processed Ti-6Al-4V scaffolds could be optimized by controlling the cell shape[146]. Shah *et al.*[147] obtained Ti-6Al-4V and CoCr scaffolds with similar architecture using EBM, as shown in Figure 8B. *In vivo* tests were performed to investigate their effects on bone tissue growth. Although similar bone formation patterns presented in the porous network, higher osteocyte density was observed at the periphery of the CoCr scaffolds, due to its more favorable biomechanical environment. These results confirmed the great potential of osseointegrated CoCr scaffolds for load-bearing applications.

Zhao *et al.*[148] fabricated Ti-6Al-4V scaffolds with cubic, G7, and rhombic dodecahedron unit cells using EBM before investigating their fatigue behavior. It was revealed that the fatigue mechanism for these scaffolds is the interaction of cyclic ratcheting and fatigue crack growth on the struts, which is closely related to the cumulative effect of buckling and bending deformation of the strut. Zhao *et al.*[149] studied the corrosion behavior of EBM-processed scaffolds, revealing a better corrosion resistance as compared to wrought scaffolds. As a permanent implant, the Ti-6Al-4V scaffolds with high anti-corrosion ability led to reduced precipitate of harmful metallic ion, such as Al and V ions, which might avoid serious complication. The cytocompatibility and osteogenesis of EBM-processed Ti-based scaffolds were also investigated[150]. Results revealed that the scaffolds supported the cell attachment and proliferation with a minimal inflammatory cytokine secretion. In addition, the scaffolds with a pore size of 640 μm exhibited better biocompatibility than those with a pore size of 1200 μm because of their larger specific surface area.

It should be noted that the electron beam utilized in EBM normally has a low resolution because the electron beam is difficult to focus. Thus, the scaffolds prepared from EBM have large surface roughness[151]. The accuracy of EBM is limited within a range of 0.3–0.4 mm, which makes it difficult to fabricate scaffolds with a small pore size. Eldesoukya *et al.*[152] evaluated the geometric deviation between the EBM processed scaffolds and the initial CAD model utilizing a digital optical microscope. It was found that the struts designed with a smaller thickness would be produced oversized, leading to a corresponding pore size reduction and higher relative density. On top of that, strut thicknesses below 0.5 mm were under the threshold of processing with EBM. Besides, the cooling process during EBM takes a long period, which significantly reduces the efficiency[153]. In comparison, EBM is limited to process conductive metal materials, whereas SLS/SLM is able to process a wide range of biomaterials, including metals, ceramics, and polymers.

3.5. SLA

SLA, also known as vat polymerization, fabricates products through selectively curing photoreactive resin[154]. Specifically, it initiates with the formulation of the photopolymer liquid in a vat. Then, an ultraviolet light radiates on the surface with designed pattern and initiates the polymerization of the photoreactive liquid, while the platform moves the parts being built downward after each new layer is cured. This step will be repeated as the entire object is constructed. After draining the excessive resin, the object with desired structure is finally obtained. In general, two kinds of polymerization reaction, including free-radical polymerization and cationic polymerization, are utilized in SLA[155,156].

In terms of irradiation type, SLA can be further divided into vector scan approach and mask projection approach, as presented in Figure 9A. In the first approach, one ultraviolet beam serves as the radiation source and projects on the liquid surface for polymerization through optics and a scanning galvanometer. However, in the second approach, the radiation source creates a large-area pattern with the aiding of a digital micromirror device, thus hardening one layer at a time. Comparatively,

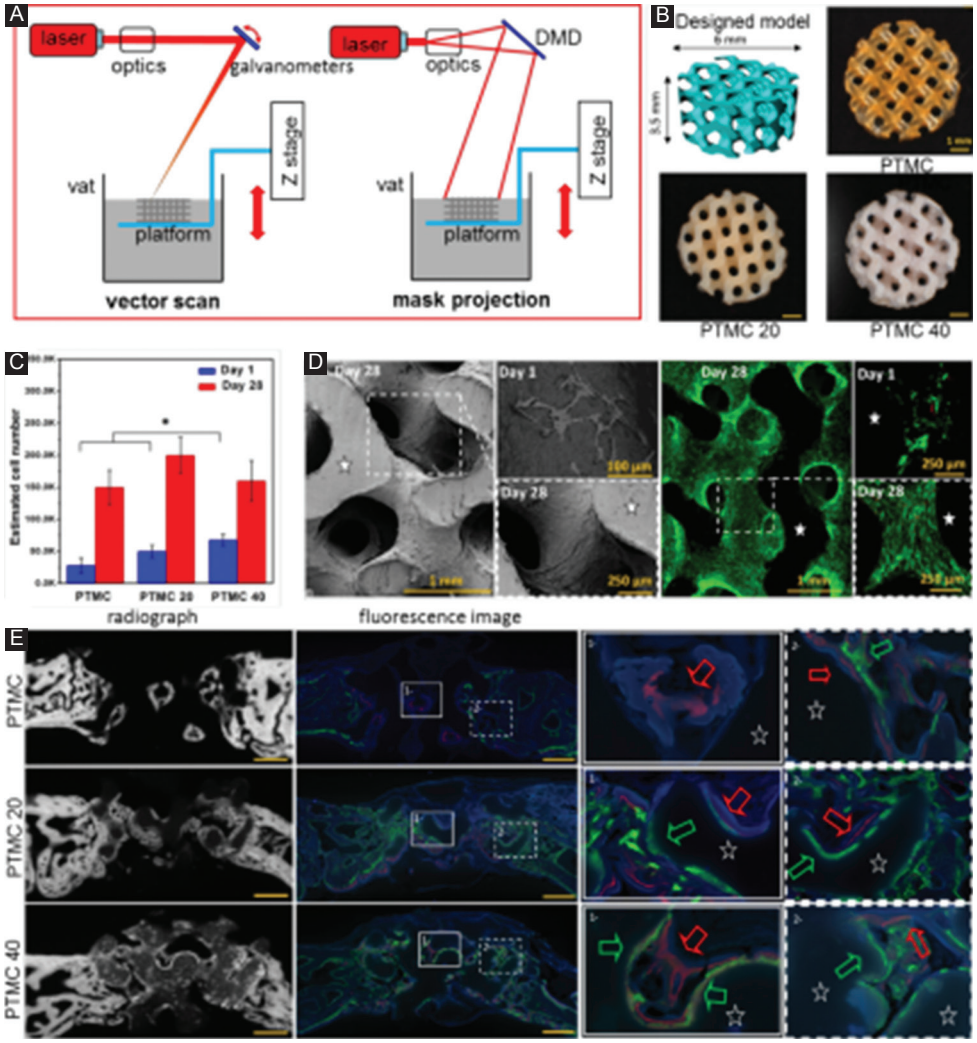

Figure 9. (**A**) A diagram for two irradiation types for stereolithography (SLA), including vector scan and mask projection. (**B**) Poly(trimethylene carbonate) (PTMC) scaffolds fabricated by SLA with various hydroxyapatite (HA) contents, with PTMC20 and PTMC40 containing 20 and 40 wt.% HA, respectively[160]. (**C**) *In vitro* cell culture on scaffolds, with (**D**) scanning electron microscope and fluorescence images showing the different cell morphologies on the scaffold. (**E**) Contact radiographs of the defects combined with fluorescence images showing the newly formed bone after implantation for 2 weeks (in green) and 4 weeks (in red).

the second method can obtain an improved building efficiency, whereas the first method can achieve a higher accuracy.

Some synthetic polymers combined with photoreactive features, good biocompatibility, and suitable mechanical properties are used in SLA. For instance, PCL was used to fabricate scaffolds by SLA[157]. Mechanical tests showed that the SLA-processed PCL scaffolds had elastic mechanical properties with Young's modulus ranging from 6.7 to 15.4 MPa. In addition, cell culture experiments confirmed its good biocompatibility. Poly(tetrahydrofuran) was also used for printed scaffolds with Young's modulus ranging from 5.7 to 27.5 MPa, bending strength ranging from 1.1 to 3.5 MPa[158], where no cytotoxicity was also showed[159]. Besides, PEG was also used in SLA to produce scaffolds with a large elastic modulus range (5.3±0.9–74.6±1.5 kPa). There are also a small number of reports on the use of SLA to build composite scaffolds for bone tissue engineering. For example, Guillaume *et al.*[160] successfully applied SLA to fabricate poly(trimethylene carbonate) (PTMC)/HA composite scaffolds, as shown in Figure 9B. The incorporated HA was enriched on the surface of scaffolds, forming a microscale structured. *In vitro* and *in vivo* experiments revealed an improved marrow stem cell differentiation and accelerated kinetic of bone healing for the microscale-structured PTMC/HA scaffolds (Figure 9C-E).

Ceramic scaffolds can also be fabricated by SLA. In general, ceramic particles are homogeneously suspended

in resin and photopolymerized in the SLA before burning up the resin and sintering the ceramics particles together. Thavornyutikarn *et al.*[161] produced bioceramic scaffolds using suspensions, which contain 41 vol.% of bioglass and 49 vol.% of an acrylate-based photopolymer resin together with 10 vol.% of a dispersing agent. The binder was removed after heating to 550°C for 3 h, and the scaffolds were then sintered at 950°C for 2 h. Du *et al.*[162] also successfully fabricated customized ceramic scaffolds using SLA based on a rabbit femoral segment model. After culturing in oscillatory perfusion for 5 days, the cells attached and proliferated homogenously on the scaffolds. Similarly, Levy *et al.*[163] successfully produced HA ceramic scaffolds for orbital floor prosthesis by SLA. Of particular note is that SLA of such a composite resin is extremely difficult, due to its significantly increased viscosity. Moreover, the particle size of the added ceramic should be less than the curing thickness, so as to avoid a damage of the processing accuracy.

Indirect method has also been reported to produce scaffolds through SLA. For example, Sabree *et al.*[164] used SLA to create an epoxy mold designed from the negative images of implants. Then, a highly loaded HA-acrylate suspension was filled into the mold. Subsequently, both the mold and the acrylic binder were removed by pyrolysis. The remaining HA scaffolds were then sintered to improve the densification rate. The obtained scaffolds possessed a porosity of approximately 42% and pore sizes of 300–600 μm. They presented an average crushing strength of 10–25 MPa, which were close to other ceramic scaffolds with similar porosity produced by different fabrication approaches. Kim *et al.* also used such an indirect method to produce HA scaffolds[165].

Compare to other AM techniques, the main advantage of SLA is that it has high accuracy and resolution. SLA using two-photon curing method can build parts with an accuracy of 200 nm[166]. Therefore, SLA is also reported to be used to prepare vascular scaffolds with a smaller pore structure. Nevertheless, the limited material use of photo resins and time-consuming post-processing remain challenges for the further application of SLA in biomedical application.

3.6. Electrospinning

In decades, electrospinning has gained intensive attention from the researchers in tissue engineering field, due to its powerful ability to fabricate scaffolds with micro- and nano-scale structure[167-169]. A typical electrospinning apparatus generally includes a capillary tube with a spinneret, a high-voltage power supply, and a collector, as shown in Figure 10A. During electrospinning, the polymer solution is extruded from the electrically conductive spinneret to obtain droplets. The high voltage is imposed between the spinneret and the grounded

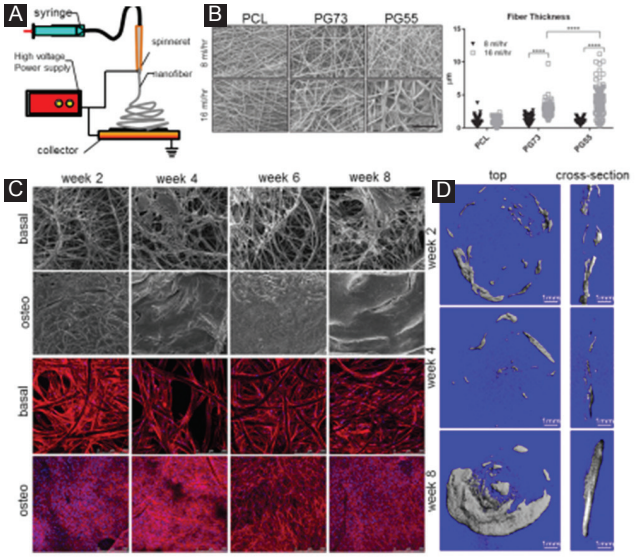

Figure 10. (**A**) A diagram showing an electrospinning setup. (B) Electrospun PCL/gelatin-blended scaffolds, and the measured fiber thickness at various parameters[179]. PG73 means the PCL/gelatin ratio of 70:30, and PG55 means the PCL/gelatin ratio of 50:50. (**C**) Confocal laser microscopy of scaffolds under basal or osteogenic conditions[177]. (**D**) Representative 3D reconstructions for the implants at 2, 4, and 8 weeks' post-implantation.

collector. Once the potential within the solution breaks through the surface tension of the obtained droplets, the polymer solution ejects from the spinneret. After the solvent evaporates, the polymer fibers are subsequently collected onto the grounded collector. As a result, a fibrous polymer scaffold with fiber diameter ranging from a 100 nm to several micrometers is constructed. Similar to FDM, electrospinning uses a nozzle to deliver the molten polymer for 3D structure construction. Thus, electrospinning is also described as "electrostatically assisted FDM"[138]. Significantly, electrospinning produces much thinner filaments by applying high voltage supply.

During electrospinning, it is of great importance to form a stable fiber, which in turn demands the polymer chains extensively entangling in the original solution. Otherwise, the solution will be ejected into a series of small droplets or aggregates into large bead-shaped fibers. From this view, low molecular weight polymers with a relative small molecular size are usually difficult to electrospin, due to their poor ability to entangle with each other. On the other hand, polymers with an extremely high molecular weight usually have a considerably increased solution viscosity, which inevitably increases the surface tension of the formed droplet-thus reducing the ability to form a jet fluid[170]. Based on the above consideration, researchers commonly introduce a second polymer to enhance the chain entanglement without an increase of the viscosity or use of amphiphilic molecules to reduce the surface tension[171].

Several thermoplastic polymers were used to fabricate electrospun scaffolds for bone tissue engineering, such as PCL[172], PLGA[173,174], and PLA[175]. For instance, Shim *et al.*[176] reported electrospun PLLA fibrous scaffolds, which were proved to be desirable substrates for cell growth and bone construction, while Vaquette *et al.*[177] produced electrospun PCL scaffolds and investigated the cell adhesion. It was observed that a dense cell sheet formed on the top and bottom of the samples cultured in osteogenic media (Figure 10C). However, microcomputed tomography analysis revealed the slow bone regeneration until implantation for 8 weeks (Figure 10D). Yao *et al.*[178] prepared 3D electrospun PCL and PCL/PLA nanofibrous scaffolds, which exhibited a high porosity of ~95.8% and interconnected and multiscale structure with pores sizes ranging from submicrometers to 300 μm. Compared to PCL scaffolds, PCL/PLA scaffolds exhibited enhanced mechanical properties and bioactivities. In fact, the synthetic nanofibrous scaffolds with relative low mechanical strength and poor ability to interact with cells have difficulty in meeting the requirements of bone repair. Thus, researchers attempted to prepare biphasic composite nanofibrous scaffolds with an improved comprehensive performance. Tan *et al.*[179] obtained PCL and gelatin-blended scaffolds by electrospun, as shown in Figure 10B. It was found that PG73 scaffold (PCL: gelatin ratio of 70:30) spun at high flow rates was more favorable for cell growth and retention. Besides, Li *et al.*[180] reported electrospun composite nanofibers composed of mesoporous silica nanoparticles and chitosan. The incorporation of mesoporous silica nanoparticles was proved to enhance the mechanical properties and promote biomineralization ability of the scaffolds. In addition, Lin *et al.*[181] reported electrospun PLGA/HAp/Zein scaffolds, which exhibited excellent ability to promote *in vivo* cartilage formation. Bagchi *et al.*[182] incorporated three different perovskite ceramic nanoparticles into PCL nanofiber, resulting in an enhanced expression of osteogenic genes. It is noted that an excess addition of nanoparticles would disrupt the formation of polymer fiber, leading to deteriorated mechanical behavior.

The electrospun fiber scaffolds also show great loading and encapsulation capacity of various drugs or small molecules because of their characteristic nanoscale morphological structure[171,183]. For electrospun nanofiber drug delivery system, it possesses greater permeability to allow shorter response time and more precise control over the release rate. Thus, a large amount of bone scaffolds containing various drugs or small molecules, such as anticancer drugs, antibiotics, polysaccharide, and proteins, was constructed to achieve a controllable drug delivery into defective bone tissues[184,185]. For example, electrospun PCL fibers were used as carriers of ketoprofen, a non-steroidal anti-inflammatory drug for local chemotherapy[186]. Kolambkar *et al.*[187] fabricated the electrospun PCL nanofibrous scaffolds, which contained a growth factor delivery system for stable release of recombinant bone morphogenetic protein-2 (rhBMP-2). It was found that the delivery system provided a consistent release of rhBMP-2 in the fibrous structure, which effectively induced the bone formation. More comprehensive review regarding the area of using electrospun nanofiber scaffolds as a drug delivery system can be seen in Wang *et al.*[171] and Bagchi *et al.*[183].

4. Post-treatments

Although the porous scaffolds fabricated by AM can achieve the analogous porous architecture of natural bone, their various properties, especially mechanical properties and biological characteristics, are commonly lower than expectation. Therefore, post-treatments are commonly needed to enhance the comprehensive performance of AM processed scaffolds so that they can reach the requirements of bone tissue repair. Summarizing the previous literature, the post-treatment technologies applied in AM-processed scaffolds can be classified into two categories, including heat treatment and surface treatment, which are fully reviewed in this chapter.

4.1. Heat Treatment

Heat treatment is a way to improve the performance by modifying the microstructure. In extrusion process, solid ceramic particles are generally mixed with a solvent to form slurry, then extruded through the nozzle, and directly built into scaffolds. Such green scaffolds inevitably have extremely loose structure and resultant poor mechanical property. Thus, the heat treatment is essential to sinter and consolidate the solid particles together, with an aim to improve the mechanical properties. Aleni *et al.*[188] used extrusion method to fabricate TiO_2 scaffolds with bentonite powder (2 wt.%) as the binder and water (35 wt.%) as the solvent. To harden the scaffolds, they were sintered at 1200–1300°C for 4 h with heating and cooling rates of 10°C/min. Mechanical tests revealed that the elastic modulus of TiO_2 scaffolds after post-heat treatment ranged from 2.08 to 5.90 GPa, which was close to that of high-density cancellous bone. Huang *et al.*[189] used HA/TCP composite ceramic slurry to fabricate scaffolds by extrusion method. HA and TCP powders were dissolved in the solvent, which consisted of 30 vol.% glycerol and 70 vol.% deionized water. After extrusion, the composite scaffolds were sintered at 400°C to burn out the glycerol before sintering at 1200°C to increase the densification rate. Results showed that scaffolds with good chemical stability had no new phase formed during

sintering. Furthermore, post-treated scaffolds with 70% porosity possessed a comparable compressive strength ~12.5 MPa to porous trabecular bone. Similar post-heat treatment was also reported to treat FDM-derived HA-based composite scaffolds[190,191].

Heat treatment has also been reported to be applied in SLS-produced scaffolds to promote the densification of the structure. It is believed that SLS-produced parts usually have a relatively low densification rate and resultant low strength due to its solid or semisolid consolidation mechanism. Therefore, a post-heat treatment is necessary for SLS-produced scaffolds, especially for high melting point ceramic scaffolds. Feng *et al.*[192] applied an isothermal heating to secondly sinter the porous HA scaffolds achieved by SLS. It was found that the isothermal heating increased the density by activating grain-boundary diffusion and grain-boundary migration. As a result, the compressive strength of scaffolds was significantly increased from 6.45 to 18.68 Mpa. Other than that, Liu *et al.*[193] used SLS to construct composites scaffolds, which exhibited a loose structure and high surface roughness. The post-heat treatment was then carried out at various temperatures ranging from 1200°C to 1400°C. After that, the compressive strength was significantly enhanced. Moreover, the surface roughness was decreased with pores shrinking.

Heat treatment is also an effective way to reduce the microstructural defects as well as the residual thermal stress. In SLM or EBM, the powders fuse and form a molten pool under the scanning of high-energy laser or electron beam, thus completing the fully melting/solidification mechanism. Nevertheless, the temperature distribution at the bottom, inner, and upper region of the molten pool is considerably different, which results in various temperature gradients in different directions. In this condition, the cooling rate in each direction varies, causing the anisotropic microstructure in the built parts. Moreover, in SLM or EBM, there is a certain remelting area at each layer, which also presents differed microstructures as compared to the region without remelting. On the other hand, SLM and EBM also involve an extremely high cooling rate, which usually leads to great residual stresses in the as-built parts. It is well known that the residual stresses considerably reduce the ductility of scaffolds. Therefore, a heat treatment is demanded to reduce the anisotropy and relieve the residual stress existing in the SLM- or EBM-deposited materials. Thone *et al.*[194] investigated the microstructure and ductility of SLM-produced Ti6Al4V after heat treatment. It was revealed that α-martensite decomposed to uniform lamellar α and β structure after heat treatment. Besides, the elongation at failure increased significantly from 1.6% to 11.6%. Similarly, Wauthle *et al.* also confirmed the considerable enhancement in ductility and homogenized microstructures of SLM-fabricated Ti6Al4V after heat treatment[195]. However, although the post-heat treatment can reduce thermal stress, it will damage its mechanical strength. The reduced strength is mainly due to the grains growth during the long period heat treatment.

4.2. Surface Treatment

Many surface treatment methods have been explored to improve the biological properties of AM-fabricated porous scaffolds. Among these, coating bioactive ceramics on scaffolds is an effective way to improve the surface bioactivity of scaffolds. Zhao *et al.*[196] achieved a uniform coating of calcium phosphate on electrospun keratin-PCL scaffolds by immersing the scaffolds into Ca^{2+} and $(PO_4)^{3-}$ solutions. Results showed that the incorporated keratin provided nucleation sites for the homogeneous deposition of calcium phosphate, which significantly facilitated the cell/matrix interactions. Luo *et al.*[197] fabricated alginate/nano-HAP composite scaffolds with a nano-HAP layer homogeneously and completely coating the surface. The surface mineralization improved the cell attachment and spreading, as well as supported a sustaining protein release compared to scaffolds without nano-HAP layer. Cell viability studies also demonstrated that polycrystalline diamond coating on TI6Al4V scaffolds promoted the attachment and proliferation of normal CHO mammalian cells and improved osseointegration[198]. Another surface coating method is electrolytic deposition. It can prepare a uniform HA layer on porous Ti scaffolds[199]. The morphology of the HA deposits could be controlled from plate-like to nanorod-like structure by altering the pulse current density. HA coating allowed more adsorption of serum proteins and further enhanced the ALP activity of MC3T3-E1 cells. Intriguingly, Chai *et al.*[200] successfully prepared CaP coating on Ti scaffolds using electrolytic deposition. However, the surface modification with brittle ceramic coating usually has an adverse effect on the elastic modulus[141]. Researchers also explored the use of a collagen layer coating on the scaffolds. It was reported that collagen coating not only improved its surface bioactivity but also improved the mechanical properties of the scaffold[201,202].

Another popular surface treatment is chemical etching, which is an effective method for modifying surface microstructures by various corrosion methods. It is well known that natural bone has a hierarchical pore structure, including macroscale, microscale, submicroscale, and nanoscale pores. Diverse scale pores act different biological functions[203]. Nevertheless, the present AM technologies are usually applied to prepare the macropore structure of bone scaffolds but come across a difficulty in fabricating microscale and submicroscale pores due to their limited resolution. To maximally mimic the hierarchical pore structure, the post-chemical etching is

proposed to construct micro- or nano-scale pore structure on AM-produced scaffolds. Amin *et al.*[204] applied both acid-alkali and alkali-acid heat treatment to functionalize the SLM-processed porous Ti scaffolds. The modified scaffolds exhibited irregular etching nano-scale pits with the size ranging from 100 to 200 nm. *In vivo* tests revealed that such features improved the apatite-forming ability, resulting in significantly larger volumes of newly formed bone within the pores of the scaffolds. Cheng *et al.*[205] treated the SLS-processed Ti-6Al-4V scaffolds through a combination of sandblasting, acid etching, and pickling. Then, a desirable multiscale micro-/nano-roughness was obtained on the surface, which was proved to enhance the osseointegration. Besides, Shuai *et al.*[206] also used chemical etching method to treat SLS-processed PLLA scaffolds. In sodium hydroxide solution, PLLA was etched into soluble polar groups through a hydrolysis reaction. Thus, well-ordered pores (1–3 μm) and smaller penetrated pores with a pore size <1 μm left on the surface. The chemical-treated scaffolds exhibited surprising bioactivity due to the formed polar groups on the surfaces. In addition, the degradation was adjustable through controlling the size and quantity of the surface pores. Ramier *et al.* reported[207] an introduction of epoxy groups on the surface of electrospun poly(3-hydroxyalkanoate) scaffolds using chemical etching. It was found that human mesenchymal stromal cells exhibited a better adhesion on the modified scaffolds as compared to the control cells. It should be taken that chemical corrosion inevitably damages the strut of scaffolds to some extent, which is possibly resulting in a negative effect on the mechanical properties of the scaffolds. It was reported that alkali treatment caused a deterioration of the mechanical strength of porous PLLA scaffold, with the compressive strength decreased by 30.1%[206]. Similar mechanical loss also occurred to porous Ti scaffolds after chemical etching[208]. Besides, researchers also applied oxygen plasma treatment to increase the surface hydrophilicity to enhance the biocompatibility[209-212].

5. Conclusions and Challenges

Currently, the demand for bone scaffolds for clinical operations is increasing rapidly. AM techniques offer unique advantages for bone scaffolds fabrication with respect to its ability to produce customized external shape and interconnected pore structure. Combining with scaffolds design and specific post-treatments, they can produce customized scaffolds with desired comprehensive performance, including suitable mechanical properties and good biological behaviors, for bone repair in a short development period. Nevertheless, the current state of AM of scaffolds for clinical application is still behind expectation. AM of bone scaffolds belongs to multidisciplinary, including manufacturing engineering, materials science, and biomedical engineering, which requires the coordination and cooperation of researchers in different fields.

In terms of porous structure, hierarchical and gradient pore structure similar to that of natural bone is the most conducive to the growth of bone tissue. The current CAD design software enables the designer to easily complete scaffolds design, but it is still not able to support the complex geometric features for scaffold modeling. In contrary, reverse modeling and mathematical modeling methods are time-consuming but exhibit powerful ability to construct complex geometric gradient features. Therefore, combining CAD design with CT imaging or mathematical modeling may help to achieve more rapid and mimic scaffold model. Bone scaffolds are also expected to meet the requirements of suitable mechanical and biological properties, including elastic modulus, stiffness, porosity, and permeability. However, there is still no definite design standard for bone scaffold design. Therefore, the application of computer-aided engineering technology in multiobjective optimization analysis of scaffold structure will become the focus of bone scaffolds design in the further investigation. Using topology optimization, the mechanical and biological performance of the scaffold can be optimized to achieve the optimal comprehensive performance. Nonetheless, the macro- and micro-integration design of porous scaffolds needs further study through topology optimization.

In terms of AM process, the AM techniques applied in bone tissue engineering are far behind the industrial application standards. Improving the accuracy and efficiency of processing should be one of the research directions in the future. The accuracy of AM built scaffolds is influenced by many factors, including models files, equipment system, and process parameters[36,213,214]. Although the post-treatment process can improve the surface accuracy, it is time-consuming and tends to reduce the efficiency. To overcome this issue, one primary task is to achieve a fundamental understanding of the affecting mechanism of the processing parameters on the formation quality. Take SLM or EBM as an example, solving the key technical issues, such as the interaction between laser beam (electron beam) and powder, the control of residual stress, and the processing stability, will unquestionably make a positive influence on improving the processing accuracy. On the other hand, nano- and micro-technology have been developing rapidly in recent years. The combination of nano- and micro-technology with AM technology may offer a great chance for improving the processing accuracy of AM-derived bone scaffolds in the near future.

From the view of material system, developing more kinds of functional material for bone tissue repair is another future research direction for AM techniques. This is because that there are very limited materials can

be used in AM techniques. The material used in AM of scaffolds should not only meet the requirements of medical applications but also need to meet the technical requirements of AM. For instance, the resins used in SLA are very limited because the resin should be a liquid that rapidly solidifies on illumination with light. What is more serious is the current SLA technique is still limited to the use of a single resin at a time. As for materials used in SLS or SLM, it should have good fluidity and thermal conductivity and the powder should have a suitable shape for powder application. In fact, powders used for SLM equipment require spherical shape and a uniform particle size distribution. To satisfy these specific requirements, it is necessary to develop the dedicated material system for AM. On the other hand, hybrid materials integrate the advantages of several materials, which may exhibit better properties as used in AM scaffolds for bone regeneration. Previous researches have confirmed that AM technology could fabricate parts with multiple materials. These compositional variations are not only expected to change their processability but also are expected to achieve better mechanical or biological properties.

There is no doubt that the application of AM scaffolds for bone repair has a bright future. Thus, multidisciplinary research will be necessary to face those challenges and fully realize the potential of AM in bone repair applications in the coming days.

Conflicts of Interest

There are no conflict of interest.

Acknowledgments

This work was supported by the following funds: (1) The Natural Science Foundation of China (51575537, 81572577, 51705540); (2) Hunan Provincial Natural Science Foundation of China (2016JJ1027); (3) The Project of Innovation-driven Plan of Central South University (2016CX023); (4) The Open-End Fund for the Valuable and Precision Instruments of Central South University; (5) The fund of the State Key Laboratory of Solidification Processing in NWPU (SKLSP201605); (6) National Postdoctoral Program for Innovative Talents (BX201700291); (7) The Project of State Key Laboratory of High Performance Complex Manufacturing, Central South University; (8) The Project of Hunan Provincial Science and Technology Plan (2017RS3008).

References

1. Gao C, Peng S, Feng P*, et al.*, 2017, Bone biomaterials and interactions with stem cells. *Bone Res.*, 5(4): 17059.
2. Currey J D, 2012, The structure and mechanics of bone. *J. Mater. Sci.*, 47(1): 41–54.
3. Heuijerjans A, Wilson W, Ito K*, et al.*, 2017, The critical size of focal articular cartilage defects is associated with strains in the collagen fibers. *Clin Biomech*, 50: 40.
4. Yang Y, Wu P, Wang Q*, et al.*, 2016, The enhancement of Mg corrosion resistance by alloying Mn and laser–melting. *Materials*, 9(4): 216.
5. Hoover S, Tarafder S, Bandyopadhyay A*, et al.*, 2017, Silver doped resorbable tricalcium phosphate scaffolds for bone graft applications. *Mater Sci Eng C Mater Biol Appl*, 79: 763–769.
6. Faroni A, Mobasseri S A, Kingham P J*, et al.*, 2015, Peripheral nerve regeneration: Experimental strategies and future perspectives. *Adv Drug Deliv Rev*, 82–83: 160–167.
7. Shau D, Patton R, Patel S*, et al.*, 2018, Synthetic mesh vs. Allograft extensor mechanism reconstruction in total knee arthroplasty – A systematic review of the literature and meta–analysis. *Knee*, 25(1): 2.
8. Wang Z, Wang C, Li C*, et al.*, 2017, Analysis of factors influencing bone ingrowth into three–dimensional printed porous metal scaffolds: A review. *J Alloys Compd*, 717: 271–285.
9. Kumar A, Mandal S, Barui S*, et al.*, 2016, Low temperature additive manufacturing of three dimensional scaffolds for bone–tissue engineering applications: Processing related challenges and property assessment. *Mater Sci Eng R*, 103: 1–39.
10. Chevalier E, Chulia D, Pouget C*, et al.*, 2008, Fabrication of porous substrates: A review of processes using pore forming agents in the biomaterial field. *J Pharm Sci*, 97(3): 1135–1154.
11. Pia G, Casnedi L, Ionta M*, et al.*, 2015, On the elastic deformation properties of porous ceramic materials obtained by pore–forming agent method. *Ceram Int*, 41(9): 11097–11105.
12. Moghadam M Z, Hassanajili S, Esmaeilzadeh F*, et al.*, 2017, Formation of porous HPCL/LPCL/HA scaffolds with supercritical CO_2 gas foaming method. *J Mech Behav Biomed Mater*, 69: 115.
13. Costantini M, Colosi C, Mozetic P*, et al.*, 2016, Correlation between porous texture and cell seeding efficiency of gas foaming and microfluidic foaming scaffolds. *Mater Sci Eng C Mater Biol Appl*, 62: 668–677.
14. Theodorou G S, Eleana K, Anna T*, et al.*, 2016, Sol–Gel derived Mg–based ceramic scaffolds doped with zinc or copper ions: Preliminary results on their synthesis, characterization, and biocompatibility. *Int J Biomater*, 2016(1–2): 3858301.
15. Ros–Tárraga P, Murciano A, Mazón P*, et al.*, 2017, New 3D stratified Si–Ca–P porous scaffolds obtained by sol–gel and polymer replica method: Microstructural, mineralogical and chemical characterization. *Ceram Int*, 43(8): 6548–6553.

16. Abdkhorsand S, Sabersamandari S, 2017, Development of nanocomposite scaffolds based on TiO_2 doped in grafted chitosan/hydroxyapatite by freeze drying method and evaluation of biocompatibility. *Int J Biol Macromol*, 101: 51–58.
17. Fereshteh Z, Fathi M, Bagri A*, et al.*, 2016, Preparation and characterization of aligned porous PCL/zein scaffolds as drug delivery systems via improved unidirectional freeze–drying method. *Mater Sci Eng C Mater Biol Appl*, 68: 613–622.
18. Janik H M, 2015, A review: Fabrication of porous polyurethane scaffolds. *Mater Sci Eng C Mater Biol Appl*, 48: 586.
19. Bose S, Ke D, Sahasrabudhe H*, et al.*, 2017, Additive manufacturing of biomaterials. *Prog Mater Sci*, 93:1-310.
20. Parthasarathy J, 2014, 3D modeling, custom implants and its future perspectives in craniofacial surgery. *Ann Maxillofac Surg*, 4(1): 9.
21. Jardini A L, Larosa M A, Bernardes L F*, et al.*, 2014, Customised titanium implant fabricated in additive manufacturing for craniomaxillofacial surgery. *Virtual Phys Prototyp*, 9(2): 115–125.
22. Avaliable from: http://www.csiro.au/en/News/News–releases/2014/3D–Heel–In–World–First–Surgery2014.
23. Song W, Chen L, Seta J*, et al.*, 2017, Corona discharge: A novel approach to fabricate three–dimensional electrospun nanofibers. *Acs Biomater Sci Eng,* 3(6): 1146–1153.
24. Hollister S J, Flanagan C L, Morrison R J*, et al.*, 2016, Integrating image–based design and 3D biomaterial printing to create patient specific devices within a design control framework for clinical translation. *Acs Biomater Sci Eng*, 2(10): 1658-1661.
25. Shuai C, Guo W, Gao C*, et al.*, 2018, An nMgO containing scaffold: Antibacterial activity, degradation properties and cell responses. *Int J Bioprint,* 4(1): 34-578.
26. He J, Xu F, Dong R*, et al.*, 2017, Electrohydrodynamic 3D printing of microscale poly (ε–caprolactone) scaffolds with multi–walled carbon nanotubes. *Biofabrication*, 9(1): 15007.
27. Guvendiren M, Molde J, Soares R*, et al.*, 2016, Designing biomaterials for 3D printing. *Acs Biomater Sci Eng*, 2(10): 1679–1693.
28. Calignano F, 2014, Design optimization of supports for overhanging structures in aluminum and titanium alloys by selective laser melting. *Mater Design*, 64(9): 203–213.
29. Yan R, Luo D, Huang H*, et al.*, 2018, Electron beam melting in the fabrication of three–dimensional mesh titanium mandibular prosthesis scaffold. *Sci Rep*, 8(1): 750.
30. Yu G Z, Chou D T, Hong D*, et al.*, 2017, Biomimetic rotated lamellar plywood motifs by additive manufacturing of metal alloy scaffolds for bone tissue engineering. *Acs Biomater Sci Eng*, 3(4): 649–657.
31. Feng J, Fu J, Shang C*, et al.*, 2018, Porous scaffold design by solid T–splines and triply periodic minimal surfaces. *Comput Methods Appl Mech Eng,* 336, 333–352.
32. Probst F A, Hutmacher D W, Müller D F*, et al.*, 2010, Calvarial reconstruction by customized bioactive implant. *Handchir Mikrochir Plast Chir*, 42(6): 369.
33. Naing M W, Chua C K, Leong K F*, et al.*, 2005, Fabrication of customised scaffolds using computer-aided design and rapid prototyping techniques. *Rapid Prototyp J*, 11(4): 249–259.
34. Ovsianikov A, Deiwick A, Vlierberghe S V*, et al.*, 2011, Laser fabrication of three–dimensional CAD scaffolds from photosensitive gelatin for applications in tissue engineering. *Biomacromolecules*, 12(4): 851–858.
35. Yu K M, Chiu W K, Yeung Y C, 2006, Toolpath generation for layer manufacturing of fractal objects. *Rapid Prototyp J*, 12(4): 214–221.
36. Sing S L, Wiria F Eand Yeong W Y, 2018, Selective laser melting of lattice structures: A statistical approach to manufacturability and mechanical behavior. *Robot Comput Integr Manuf*, 49: 170–180.
37. Duan B, Cheung W, Land W M, 2011, Optimized fabrication of Ca–P/PHBV nanocomposite scaffolds via selective laser sintering for bone tissue engineering. *Biofabrication*, 3(1): 15001.
38. Melchels F P, Bertoldi K, Gabbrielli R*, et al.*, 2010, Mathematically defined tissue engineering scaffold architectures prepared by stereolithography. *Biomaterials*, 31(27): 6909.
39. Sercombe T B, Xu X, Challis V J*, et al.*, 2015, Failure modes in high strength and stiffness to weight scaffolds produced by selective laser melting. *Mater Des*, 67: 501–508.
40. Murr L E, Gaytan S M, Medina F*, et al.*, 2010, Next–generation biomedical implants using additive manufacturing of complex, cellular and functional mesh arrays. *Philos Trans*, 368(1917): 1999.
41. Cheah C M, Chua C K, Leong K F*, et al.*, 2004, Automatic algorithm for generating complex polyhedral scaffold structures for tissue engineering. *Tissue Eng*, 10(4): 595–610.
42. Lu G, Xu S, Yan Q S*, et al.*, 2013, Study on dimension change law from CAD model to prototype of rapid investment casting based on selective laser sintering. *Adv Mater Res*, 774–776(774–776): 1046–1050.
43. Florczyk S J, Simon M, Juba D*, et al.*, 2017, A bioinformatics 3D cellular morphotyping strategy for assessing biomaterial scaffold niches. *Acs Biomater Sci Eng*, 3(10): 2302-2313.

44. Kerativitayanan P, Tatullo M, Khariton M*, et al.*, 2017, Nanoengineered osteoinductive and elastomeric scaffolds for bone tissue engineering. *Acs Biomater Sci Eng*, 3(4): 590–600.
45. Thomas R C, Vu P, Shan P M*, et al.*, 2017, Sacrificial crystal templated hyaluronic acid hydrogels as biomimetic 3D tissue scaffolds for nerve tissue regeneration. *Acs Biomater Sci Eng*, 3(7): 1172–1174.
46. Altamimi A A, Fernandes P R A, Peach C*, et al.*, 2017, Metallic bone fixation implants: A novel design approach for reducing the stress shielding phenomenon. *Virtual Phys Prototyp*, 12(2): 141–151.
47. Osanov J K, 2016, Topology optimization for architected materials design. *Ann Rev Mater Res*, 46(1): 211–233.
48. Guest J Kand Prévost J H, 2007, Design of maximum permeability material structures. *Comput Methods Appl Mech Eng*, 196(4–6): 1006–1017.
49. Guest J, Kand P J, 2006, Optimizing multifunctional materials: Design of microstructures for maximized stiffness and fluid permeability. *Int J Solids Struct*, 43(22): 7028–7047.
50. Sturm S, Zhou S, Mai Y W*, et al.*, 2010, On stiffness of scaffolds for bone tissue engineering – A numerical study. *J Biomech*, 43(9): 1738–1744.
51. Huang, X X, 2010, *Evolutionary Topology Optimization of Continuum Structures: Methods and Applications*. Hoboken, New Jersey: Wiley.
52. Huang X, Xie Y M, 2011, Topological design of microstructures of cellular materials for maximum bulk or shear modulus. *Comput Mater Sci*, 50(6): 1861–1870.
53. Osher S, Sethian J A, 1988, Fronts propagating with curvature–dependent speed: Algorithms based on Hamilton–Jacobi formulations. *J Comput Phys*, 79(1): 12–49.
54. Li Q Z, 2008, *A Variational Level set Method for the Topology Optimization of Steady–State Navier–Stokes Flow*. USA: Academic Press Professional, Inc.
55. Challis V, Guest J K, 2010, Level set topology optimization of fluids in stokes flow. *Int J Num Methods Eng*, 79(10): 1284–1308.
56. Takezawa A, Kobashi M, Takezawa A*, et al.*, 2017, Design methodology for porous composites with tunable thermal expansion produced by multi–material topology optimization and additive manufacturing. *Compos Part B Eng*, 131: 1-283.
57. Hollister S J, Levy R A, Chu T M*, et al.*, 2000, An image–based approach for designing and manufacturing craniofacial scaffolds. *Int J Oral Maxillofac Surg*, 29(1): 67–71.
58. Giannitelli S M, Accoto D, Trombetta M*, et al.*, 2014, Current trends in the design of scaffolds for computer – Aided tissue engineering. *Acta Biomater*, 10(2): 580–594.
59. Sun W, Starly B, Nam J*, et al.*, 2005, Bio–CAD modeling and its applications in computer–aided tissue engineering. *Comput Aided Des*, 37(11): 1097–1114.
60. Hollister S J, Chu T M, Guldberg R E*, et al.*, 2002, *Image Based Design and Manufacture of Scaffolds for Bone Reconstruction*. IUTAM Symposium on Synthesis in Bio Solid Mechanics. pp163-174.
61. Hollister S J, 2005, Porous scaffold design for tissue engineering. *Nat Mater*, 4(7): 518–524.
62. Podshivalov L, Gomes C M, Zocca A*, et al.*, 2013, Design, analysis and additive manufacturing of porous structures for biocompatible micro–scale scaffolds -. *Procedia Cirp*, 5(1): 247–252.
63. Meyer U, Runte C, Dirksen D*, et al.*, 2003, *Image–Based Biomimetric Approach to Design and Fabrication of Tissue Engineered Bone.* Cars 2003. Computer Assisted Radiology and Surgery. Proceedings of the International Congress and Exhibition, London. pp726–732.
64. Pattanayak D K, Fukuda A, Matsushita T*, et al.*, 2011, Bioactive ti metal analogous to human cancellous bone: Fabrication by selective laser melting and chemical treatments. *Acta Biomater*, 7(3): 1398–1406.
65. Terasaki O, 2005, Band structure of the P, D, and G surfaces. *Phys Rev B*, 72(8):085459.
66. Lai M, Kulak A N, Law D*, et al.*, 2007, Profiting from nature: macroporous copper with superior mechanical properties. *Chem Commun*, 34(34): 3547–3549.
67. Robb R A, 2005, *Schwarz Meets Schwann: Design and Fabrication of Biomorphic and Durataxic Tissue Engineering Scaffolds*. Palm Springs, CA, USA: Medical Image Computing and Computer–assisted Intervention–miccai, International Conference. pp794–801.
68. Kapfer S C, Hyde S T, Mecke K*, et al.*, 2011, Minimal surface scaffold designs for tissue engineering. *Biomaterials*, 32(29): 6875–6882.
69. Melchels F W, Barradas A M, Blitterswijk C A*, et al.*, 2010, Effects of the architecture of tissue engineering scaffolds on cell seeding and culturing. *Acta Biomater*, 6(11): 4208–4217.
70. Yang N, Quan Z, Zhang D*, et al.*, 2014, Multi–morphology transition hybridization CAD design of minimal surface porous structures for use in tissue engineering. *Comput Aided Des*, 56(11): 11–21.
71. Yang N, Wang S, Gao L*, et al.*, 2017, Building implicit–surface–based composite porous architectures. *Compos Struct*, 173: 35–43.
72. Zhou K Y, 2014, Effective method for multi–scale gradient

porous scaffold design and fabrication. *Mater Sci Eng C Mater Biol Appl*, 43: 502–505.

73. Yang N, Zhang D T, 2015, Novel real function based method to construct heterogeneous porous scaffolds and additive manufacturing for use in medical engineering. *Med Eng Phys*, 37(11): 1037–1046.
74. Yang N, Du C F, Wang S*, et al.*, 2016, Mathematically defined gradient porous materials. *Mater Lett*, 173: 136–140.
75. Yoo D J, 2011, Porous scaffold design using the distance field and triply periodic minimal surface models. *Biomaterials*, 32(31): 7741.
76. Yoo D J, 2013, Heterogeneous porous scaffold design using the continuous transformations of triply periodic minimal surface models. *Int J Precis Eng Manuf*, 14(10): 1743–1753.
77. Yoo D, Kim K H, 2015, An advanced multi–morphology porous scaffold design method using volumetric distance field and beta growth function. *Int J Precis Eng Manuf*, 16(9): 2021–2032.
78. Yang N, Zhou K G, 2015, Simple method to generate and fabricate stochastic porous scaffolds. *Mater Sci Eng C*, 56: 444–450.
79. Roberts A, Garboczi E J, 2001, Elastic moduli of model random three–dimensional closed–cell cellular solids. *Acta Mater*, 49(2): 189–197.
80. Okabe A, Boots B, Sugihara K*, et al.*, 2001, *Spatial Tessellations: Concepts and Applications of Voronoi Diagrams*. New York, NY: John Wiley & Sons, Inc.
81. Kou X, Tan S T, 2010, A simple and effective geometric representation for irregular porous structure modeling. *Comput Aided Des*, 42(10): 930–941.
82. Kou X Y, Tan S T, 2012, Microstructural modelling of functionally graded materials using stochastic voronoi diagram and B–Spline representations. *Int J Comput Integr Manuf*, 25(2): 177–188.
83. Chow H N, Tan S T, Sze W S, 2007, Layered modeling of porous structures with voronoi diagrams. *Comput Aided Des Appl*, 4(1–4): 321–330.
84. Fantini M, Curto M, Crescenzio F D, 2016, A method to design biomimetic scaffolds for bone tissue engineering based on voronoi lattices. *Virtual Phys Prototyp*, 11(2): 77–90.
85. Curto M F, 2017, Interactive design and manufacturing of a voronoi–based biomimetic bone scaffold for morphological characterization. *Int J Interact Des Manuf*, 6: 1–12.
86. Gómez S, Vlad M D, López J*, et al.*, 2016, Design and properties of 3D scaffolds for bone tissue engineering. *Acta Biomater*, 42: 341–350.
87. Wang G, Shen L, Zhao J*, et al.*, 2018, Design and compressive behavior of controllable irregular porous scaffolds: Based on voronoi–tessellation and for additive manufacturing. *Acs Biomater Sci Eng*, 4(2): 719–727.
88. Tumbleston J R, Shirvanyants D, Ermoshkin N*, et al.*, 2015, Continuous liquid interface production of 3D objects. *Science*, 347(6228): 1349–1352.
89. Xing J–F, Zheng M–Land Duan X–M, 2015, Two–photon polymerization microfabrication of hydrogels: an advanced 3D printing technology for tissue engineering and drug delivery. *Chemical Society Reviews*, 44(15): 5031–5039.
90. Yu T, Richards D J, Trusk T C*, et al.*, 2014, 3D Printing facilitated scaffold–free tissue unit fabrication. *Biofabrication*, 6(2): 24111.
91. Pourchet L J, Thepot A, Albouy M*, et al.*, 2016, Human skin 3D bioprinting using scaffold–free approach. *Adv Healthc Mater*, 6(4): 1601101.
92. Cervera G B, Lombera G, 1999, Numerical prediction of temperature and density distributions in selective laser sintering processes. *Rapid Prototyp J*, 5(1): 21–26.
93. Gu D C, 2016, Effect of metallurgical defect and phase transition on geometric accuracy and wear resistance of iron–based parts fabricated by selective laser melting. *J Mater Res*, 31(10): 1477–1490.
94. Senatov F, Niaza K, Zadorozhnyy M Y*, et al.*, 2016, Mechanical properties and shape memory effect of 3D–printed PLA–based porous scaffolds. *J Mech Behav Biomed Mater*, 57: 139–148.
95. Jezierski A, Rennie K, Zurakowski B*, et al.*, 2014, Neuroprotective effects of GDNF–expressing human amniotic fluid cells. *Stem Cell Rev Rep*, 10(2): 251–268.
96. Shuai C, Li Y, Feng P*, et al.*, 2018, Positive feedback effects of Mg on the hydrolysis of poly–l–lactic acid (PLLA): Promoted degradation of PLLA scaffolds. *Polym Test*, 68: 27–33.
97. Yang L, Li J, Jin Y*, et al.*, 2015, *In vitro* enzymatic degradation of the cross–linked poly (ε–caprolactone) implants. *Polym Degrad Stab*, 112: 10–19.
98. Du Y, Liu H, Yang Q*, et al.*, 2017, Selective laser sintering scaffold with hierarchical architecture and gradient composition for osteochondral repair in rabbits. *Biomaterials*, 137: 37.
99. Du Y, Liu H, Shuang J*, et al.*, 2015, Microsphere–based selective laser sintering for building macroporous bone scaffolds with controlled microstructure and excellent biocompatibility. *Colloids Surf B Biointerfaces*, 135: 81.
100. Kumaresan T, Gandhinathan R, Ramu M*, et al.*, 2016, Design, analysis and fabrication of polyamide/hydroxyapatite porous

structured scaffold using selective laser sintering method for bio–medical applications. *J Mech Sci Technol*, 30(11): 5305–5312.

101. Shuai C, Gao C, Nie Y*, et al.*, 2011, Structure and properties of nano–hydroxypatite scaffolds for bone tissue engineering with a selective laser sintering system. *Nanotechnology*, 22(28): 285703.
102. Shuai C, Li P, Liu J*, et al.*, 2013, Optimization of TCP/HAP ratio for better properties of calcium phosphate scaffold via selective laser sintering. *Mater Charact*, 77(3): 23–31.
103. Liu J, Hu H, Li P*, et al.*, 2013, Fabrication and characterization of porous 45S5 glass scaffolds via direct selective laser sintering. *Mater Manuf Process*, 28(6): 610–615.
104. Sing S L, Yeong W Y, Wiria F E*, et al.*, 2017, Direct selective laser sintering and melting of ceramics: A review. *Rapid Prototyp J*, 23(3): 611–623.
105. Liu J, Gao C, Feng P*, et al.*, 2015, A bioactive glass nanocomposite scaffold toughed by multi–wall carbon nanotubes for tissue engineering. *J Ceram Soc Jpn*, 123(1438): 485–491.
106. Gao C, Pei F, Peng S*, et al.*, 2017, Carbon nanotubes, graphene and boron nitride nanotubes reinforced bioactive ceramics for bone repair. *Acta Biomater*, 61: 1.
107. Järvenpää A, Karjalainen P, Mäntyjärvi K, 2012, Passive laser assisted bending of ultra–high strength steels. *Adv Mater Res*, 418–420: 1542–1547.
108. Gao C, Liu T, Shuai C*, et al.*, 2014, Enhancement mechanisms of graphene in nano–58S bioactive glass scaffold: Mechanical and biological performance. *Sci Rep*, 4(4): 4712.
109. Duan S, Feng P, Gao C*, et al.*, 2015, Microstructure evolution and mechanical properties improvement in liquid–phase–sintered hydroxyapatite by laser sintering. *Materials*, 8(3): 1162–1175.
110. Liu D, Zhuang J, Shuai C*, et al.*, 2013, Mechanical properties' improvement of a tricalcium phosphate scaffold with poly–l–lactic acid in selective laser sintering. *Biofabrication*, 5(2): 25005.
111. Gu D, Hagedorn Y C, Meiners W*, et al.*, 2012, Densification behavior, microstructure evolution, and wear performance of selective laser melting processed commercially pure titanium. *Acta Mater*, 60(9): 3849–3860.
112. Čapek J, Machová M, Fousová M*, et al.*, 2016, Highly porous, low elastic modulus 316L stainless steel scaffold prepared by selective laser melting. *Mater Sci Eng C*, 69: 631–639.
113. Weißmann V, Bader R, Hansmann H*, et al.*, 2016, Influence of the structural orientation on the mechanical properties of selective laser melted Ti6Al4V open–porous scaffolds. *Mater Des*, 95: 188–197.
114. Wang L, Kang J, Sun C*, et al.*, 2017, Mapping porous microstructures to yield desired mechanical properties for application in 3D printed bone scaffolds and orthopaedic implants. *Mater Des*, 133: 62–68.
115. Shah F A, Snis A, Matic A*, et al.*, 2016, 3D printed Ti6Al4V implant surface promotes bone maturation and retains a higher density of less aged osteocytes at the bone–implant interface. *Acta Biomater*, 30: 357–367.
116. Yang Y, Guo X, He C*, et al.*, 2018, Regulating degradation behavior by incorporating mesoporous silica for Mg bone implants. *Acs Biomater Sci Eng*, 4(3): 1046–1054.
117. Deng Y, Yang Y, Gao C*, et al.*, 2018, Mechanism for corrosion protection of β–TCP reinforced ZK60 via laser rapid solidification. *Int J Bioprint*, 4(1): 124.
118. Shuai C, Xue L, Gao C*, et al.*, 2018, Selective laser melting of Zn–Ag alloys for bone repair: Microstructure, mechanical properties and degradation behaviour. *Virtual Phys Prototyp,* 13(3): 146-154.
119. Yang Y, Yuan F, Gao C*, et al.*, 2018, A combined strategy to enhance the properties of Zn by laser rapid solidification and laser alloying. *J Mech Behav Biomed Mater*, 82: 51–60.
120. Sing S L, An J, Yeong W Y*, et al.*, 2016, Laser and electron–beam powder–bed additive manufacturing of metallic implants: A review on processes, materials and designs. *J Orthop Res*, 34(3): 369–385.
121. Shuai C, Yang Y, Wu P*, et al.*, 2017, Laser rapid solidification improves corrosion behavior of Mg–Zn–Zr alloy. *J Alloys Comp*, 691: 961–969.
122. Shuai C, He C, Feng P*, et al.*, 2017, Biodegradation mechanisms of selective laser–melted Mg–xAl–Zn alloy: Grain size and intermetallic phase. *Virtual Phys Prototyp*, 13(2): 1–11.
123. Yang Y, Wu P, Lin X*, et al.*, 2016, System development, formability quality and microstructure evolution of selective laser–melted magnesium. *Virtual Phys Prototyp*, 11(3): 173–181.
124. Li Y, Zhou J, Pavanram P*, et al.*, 2018, Additively manufactured biodegradable porous magnesium. *Acta Biomater,* 67: 378–392.
125. Grasso M, Demir A, Previtali B*, et al.*, 2018, *In situ* monitoring of selective laser melting of zinc powder via infrared imaging of the process plume. *Robot Comput Integr Manuf*, 49: 229–239.
126. Wen P, Jauer L, Voshage M*, et al.*, 2018, Densification behavior of pure Zn metal parts produced by selective laser melting for manufacturing biodegradable implants. *J Mater*

Process Technol, 258: 128–137.

127. Demir A G, Monguzzi L, Previtali B, 2017, Selective laser melting of pure Zn with high density for biodegradable implant manufacturing. *Add Manuf*, 15: 20–28.
128. Montani M, Demir A G, Mostaed E*, et al.*, 2017, Processability of pure Zn and pure Fe by SLM for biodegradable metallic implant manufacturing. *Rapid Prototyp J*, 23(3): 514–523.
129. Hou Y, Jia G, Yue R*, et al.*, 2018, Synthesis of biodegradable Zn–based scaffolds using NaCl templates: Relationship between porosity, compressive properties and degradation behavior. *Mater Charact*, 137: 305–315.
130. Hutmacher D W, 2000, Scaffolds in tissue engineering bone and cartilage. *Biomaterials*, 21(24): 2529–2543.
131. Zhou C, Yang K, Wang K*, et al.*, 2016, Combination of fused deposition modeling and gas foaming technique to fabricated hierarchical macro/microporous polymer scaffolds. *Mater Des*, 109: 415–424.
132. Tellis B C, Szivek J A, Bliss C L*, et al.*, 2008, Trabecular scaffolds created using micro CT guided fused deposition modeling. *Mater Sci Eng C*, 28(1): 171–178.
133. Kosorn W, Sakulsumbat M, Uppanan P*, et al.*, 2017, PCL/PHBV blended three dimensional scaffolds fabricated by fused deposition modeling and responses of chondrocytes to the scaffolds. *J Biomed Mater Res Part B Appl Biomater*, 105(5): 1141.
134. De S R, D'Amora U, Russo T*, et al.*, 2015, 3D fibre deposition and stereolithography techniques for the design of multifunctional nanocomposite magnetic scaffolds. *J Mater Sci Mater Med*, 26(10): 250.
135. Vaezi M, Yang S, 2015, Extrusion–based additive manufacturing of PEEK for biomedical applications. *Virtual Phys Prototyp*, 10(3): 123–135.
136. Rinaldi M, Ghidini T, Cecchini F*, et al.*, 2018, Additive layer manufacturing of poly (ether ether ketone) via FDM. *Compos Part B Eng*, 145: 162-172.
137. Shim J H, Won J Y, Sung S J*, et al.*, 2015, Comparative efficacies of a 3D–printed PCL/PLGA/β–TCP membrane and a titanium membrane for guided bone regeneration in beagle dogs. *Polymers*, 7(10): 2061–2077.
138. Youssef A, Hollister S J, Dalton P D, 2017, Additive manufacturing of polymer melts for implantable medical devices and scaffolds. *Biofabrication*, 9(1): 12002.
139. Xu N, Ye X, Wei D*, et al.*, 2014, 3D artificial bones for bone repair prepared by computed tomography–guided fused deposition modeling for bone repair. *Acs Appl Mater Interfaces*, 6(17): 14952–14963.
140. Kim J, Mcbride S, Tellis B*, et al.*, 2012, Rapid–prototyped PLGA/β–TCP/hydroxyapatite nanocomposite scaffolds in a rabbit femoral defect model. *Biofabrication*, 4(2): 25003.
141. Poh P S, Hutmacher D W, Holzapfel B M*, et al.*, 2016, *In vitro* and *in vivo* bone formation potential of surface calcium phosphate–coated polycaprolactone and polycaprolactone/bioactive glass composite scaffolds. *Acta Biomater*, 30: 319–333.
142. Frazier W E, 2014, Metal additive manufacturing: A review. *J Mater Eng Perform*, 23(6): 1917–1928.
143. Liang Hand Harris R, 2008, *Customised Implants for Bone Replacement and Growth*. US: Springer.
144. Ataee A, Li Y, Fraser D*, et al.*, 2018, Anisotropic Ti–6Al–4V gyroid scaffolds manufactured by electron beam melting (EBM) for bone implant applications. *Mater Des*, 137: 1-480.
145. Surmeneva M, Surmenev R, Chudinova E*, et al.*, 2017, Fabrication of multiple–layered gradient cellular metal scaffold via electron beam melting for segmental bone reconstruction. *Mater Des,* 133: 195-204.
146. Li S J, Xu Q S, Wang Z*, et al.*, 2014, Influence of cell shape on mechanical properties of Ti–6Al–4V meshes fabricated by electron beam melting method. *Acta Biomater*, 10(10): 4537–4547.
147. Shah F A, Omar O, Suska F*, et al.*, 2016, Long–term osseointegration of 3D printed CoCr constructs with an interconnected open–pore architecture prepared by electron beam melting. *Acta Biomater*, 36: 296–309.
148. Zhao S, Li S J, Hou W T*, et al.*, 2016, The influence of cell morphology on the compressive fatigue behavior of Ti–6Al–4V meshes fabricated by electron beam melting. *J Mech Behav Biomed Mater*, 59: 251–264.
149. Zhao B, Wang H, Qiao N*, et al.*, 2016, Corrosion resistance characteristics of a Ti–6Al–4V alloy scaffold that is fabricated by electron beam melting and selective laser melting for implantation *in vivo*. *Mater Sci Eng C*, 70(Pt 1): 832–841.
150. Lv J, Jia Z, Li J*, et al.*, 2015, Electron beam melting fabrication of porous Ti6Al4V scaffolds: Cytocompatibility and osteogenesis. *Adv Eng Mater*, 17(9): 1391–1398.
151. Algardh J K, Horn T, West H*, et al.*, 2016, Thickness dependency of mechanical properties for thin–walled titanium parts manufactured by electron beam melting (EBM) ®;∗. *Add Manuf*, 12: 45–50.
152. Eldesouky I, Harrysson O, West H*, et al.*, 2017, Electron beam melted scaffolds for orthopedic applications. *Add Manuf,* 17: 169-175.
153. Rännar L E, Gustafson C Gand Glad A, 2008, Efficient cooling with tool inserts manufactured by electron beam melting. *Rapid Prototyp J*, 13(3): 128–135.

154. Palaganas N, Mangadlao J, De A L*, et al.*, 2017, 3D printing of photocurable cellulose nanocrystal composite for fabrication of complex architectures via stereolithography. *Acs Appl Mater Interfaces*, 9(39): 34314–34324.

155. Wan Q, Tian J, Liu M*, et al.*, 2015, Surface modification of carbon nanotubes via combination of mussel inspired chemistry and chain transfer free radical polymerization. *Appl Surf Sci*, 346: 335–341.

156. Li B, Hou W, Sun J*, et al.*, 2015, Tunable functionalization of graphene oxide sheets through surface–initiated cationic polymerization. *Macromolecules*, 48(4): 994–1001.

157. Elomaa L, Teixeira S, Hakala R, *et al.*, 2011, Preparation of poly(ε–caprolactone)–based tissue engineering scaffolds by stereolithography. *Acta Biomater*, 7(11): 3850–3856.

158. Hockaday L A, Kang K H, Colangelo N W*, et al.*, 2012, Rapid 3D printing of anatomically accurate and mechanically heterogeneous aortic valve hydrogel scaffolds. *Biofabrication*, 4(3): 35005.

159. Meyer W, Engelhardt S, Novosel E*, et al.*, 2012, Soft polymers for building up small and smallest blood supplying systems by stereolithography. *J Funct Biomater*, 3(2): 257–268.

160. Guillaume O, Geven M A, Sprecher C M*, et al.*, 2017, Surface–enrichment with hydroxyapatite nanoparticles in stereolithography–fabricated composite polymer scaffolds promotes bone repair. *Acta Biomater*, 54: 386-398.

161. Thavornyutikarn B, Tesavibul P, Sitthiseripratip K*, et al.*, 2017, Porous 45S5 bioglass®–based scaffolds using stereolithography: Effect of partial pre–sintering on structural and mechanical properties of scaffolds. *Mater Sci Eng C Mater Biol Appl*, 75: 1281.

162. Du D, Asaoka T, Ushida T*, et al.*, 2014, Fabrication and perfusion culture of anatomically shaped artificial bone using stereolithography. *Biofabrication*, 6(4): 45002.

163. Levy R A, Chu T M, Halloran J W*, et al.*, 1997, CT–generated porous hydroxyapatite orbital floor prosthesis as a prototype bioimplant. *Ajnr Am J Neuroradiol*, 18(8): 1522–1525.

164. Sabree I, Gough J E, Derby B, 2015, Mechanical properties of porous ceramic scaffolds: Influence of internal dimensions. *Ceram Int*, 41(7): 8425–8432.

165. Kim J Y, Jin W L, Lee S J*, et al.*, 2007, Development of a bone scaffold using HA nanopowder and micro–stereolithography technology. *Microelectronic Eng*, 84(5–8): 1762–1765.

166. Melchels F P, Feijen J, Grijpma D W, 2010, A review on stereolithography and its applications in biomedical engineering. *Biomaterials*, 31(24): 6121–6130.

167. Sun B, Long Y Z, Zhang H D*, et al.*, 2014, Advances in three–dimensional nanofibrous macrostructures via electrospinning. *Prog Polym Sci*, 39(5): 862–890.

168. Hochleitner G, JãNgst T, Brown T D*, et al.*, 2015, Additive manufacturing of scaffolds with sub–micron filaments via melt electrospinning writing. *Biofabrication*, 7(3): 35002.

169. Tian L, Prabhakaran M P, Hu J*, et al.*, 2016, Synergistic effect of topography, surface chemistry and conductivity of the electrospun nanofibrous scaffold on cellular response of PC12 cells. *Colloids Surf B Biointerfaces*, 145: 420–429.

170. Wang P, Wang Y, Tong L, 2013, Functionalized polymer nanofibers: A versatile platform for manipulating light at the nanoscale. *Light Sci Appl*, 2(10): e102.

171. Repanas A, Andriopoulou S, Glasmacher B, 2016, The significance of electrospinning as a method to create fibrous scaffolds for biomedical engineering and drug delivery applications. *J Drug Deliv Sci Technol*, 31: 137–146.

172. Cipitria A, 2011, Design, fabrication and characterization of PCL electrospun scaffolds - A review. *J Mater Chem*, 21(26): 9419–9453.

173. Luu Y K, Kim K, Hsiao B S*, et al.*, 2003, Development of a nanostructured DNA delivery scaffold via electrospinning of PLGA and PLA–PEG block copolymers. *J Controll Release*, 89(2): 341–353.

174. Brown J H, Das P, Divito M D*, et al.*, 2018, Nanofibrous PLGA electrospun scaffolds modified with Type I collagen influence hepatocyte function and support viability *in vitro*. *Acta Biomater*, 73: 217–227.

175. Valente T A M, Silva D M, Gomes P S*, et al.*, 2016, Effect of sterilization methods on electrospun poly (lactic acid) (PLA) fiber alignment for biomedical applications. *Acs Appl Mater Interfaces*, 8(5): 3241.

176. Shim I K, Mi R J, Kim K H*, et al.*, 2010, Novel three-dimensional scaffolds of poly (L-lactic acid) microfibers using electrospinning and mechanical expansion: Fabrication and bone regeneration. *J Biomed Mater Res Part B Appl Biomater*, 95B(1): 150–160.

177. Vaquette C, Ivanovski S, Hamlet S M*, et al.*, 2013, Effect of culture conditions and calcium phosphate coating on ectopic bone formation. *Biomaterials*, 34(22): 5538–5551.

178. Yao Q, Cosme J G, Xu T*, et al.*, 2016, Three dimensional electrospun PCL/PLA blend nanofibrous scaffolds with significantly improved stem cells osteogenic differentiation and cranial bone formation. *Biomaterials*, 115: 115.

179. Tan R P, Chan A, Lennartsson K*, et al.*, 2018, Integration of induced pluripotent stem cell–derived endothelial cells with polycaprolactone/gelatin–based electrospun scaffolds for enhanced therapeutic angiogenesis. *Stem Cell Res Ther*, 9(1): 70.

180. Li K, Sun H, Sui H, *et al.*, 2015, Composite mesoporous silica nanoparticle/chitosan nanofibers for bone tissue engineering. *Rsc Adv*, 5(23): 17541–17549.
181. Yong, D, 2015, *In vitro* and *in vivo* evaluation of the developed PLGA/HAp/Zein scaffolds for bone–cartilage interface regeneration. *Biomedical and Environmental Sciences*, 28(1): 1.
182. Bagchi A, Meka S R, Rao B N, *et al.*, 2014, Perovskite ceramic nanoparticles in polymer composites for augmenting bone tissue regeneration. *Nanotechnology*, 25(48): 485101.
183. Rezvani Z, Venugopal J R, Urbanska A M, *et al.*, 2016, A bird's eye view on the use of electrospun nanofibrous scaffolds for bone tissue engineering: Current state–of–the–art, emerging directions and future trends. *Nanomedicine*, 12(7): 2181–2200.
184. Min S K, Kim J H, Singh R K, *et al.*, 2015, Therapeutic–designed electrospun bone scaffolds: Mesoporous bioactive nanocarriers in hollow fiber composites to sequentially deliver dual growth factors. *Acta Biomater*, 16(1): 103–116.
185. Rogina A, 2014, Electrospinning process: Versatile preparation method for biodegradable and natural polymers and biocomposite systems applied in tissue engineering and drug delivery. *Appl Surf Sci*, 296(8): 221–230.
186. Kenawy E, Abdelhay F I, Elnewehy M H, *et al.*, 2015, Processing of polymer nanofibers through electrospinning as drug delivery systems. *Mater ChemPhys*, 113(1): 296–302.
187. Kolambkar Y M, Dupont K M, Boerckel J D, *et al.*, 2011, An alginate–based hybrid system for growth factor delivery in the functional repair of large bone defects. *Biomaterials*, 32(1): 65.
188. Aleni A H, Ituarte I F, Mohite A, *et al.*, 2017, Comparing stiffness of solid and scaffold nano–TiO 2 structures produced by material extrusion method. *Ceram Int*, 44(2): 2231-2239.
189. Huang W, Zhang X, Wu Q, *et al.*, 2013, Fabrication of HA/β-TCP scaffolds based on micro-syringe extrusion system. *Rapid Prototyp J*, 19(5): 319–326.
190. Zhou K, Dong C, Zhang X, *et al.*, 2015, Preparation and characterization of nanosilver–doped porous hydroxyapatite scaffolds. *Ceram Int*, 41(1): 1671–1676.
191. Chen Z, Zhang X, Yang Y, *et al.*, 2017, Fabrication and characterisation of 3D complex hydroxyapatite scaffolds with hierarchical porosity of different features for optimal bioactive performance. *Ceram Int*, 43(1): 336–344.
192. Feng P, Niu M, Gao C, *et al.*, 2014, A novel two–step sintering for nano–hydroxyapatite scaffolds for bone tissue engineering. *Sci Rep*, 4: 5599.
193. Liu F H, 2014, Synthesis of biomedical composite scaffolds by laser sintering: Mechanical properties and *in vitro* bioactivity evaluation. *Appl Surf Sci*, 297(297): 1–8.
194. Thöne M, Leuders S, Riemer A, *et al.*, 2012, Influence of Heat–Treatment on Selective Laser Melting Products – e.g. Ti6Al4V. Austin: Annual International Solid Freeform Fabrication Symposium.
195. Wauthle R, Vrancken B, Beynaerts B, *et al.*, 2015, Effects of build orientation and heat treatment on the microstructure and mechanical properties of selective laser melted Ti6Al4V lattice structures. *Add Manuf*, 5: 77–84.
196. Zhao X, Lui Y S, Choo C K, *et al.*, 2015, Calcium phosphate coated keratin–PCL scaffolds for potential bone tissue regeneration. *Mater Sci Eng C*, 49: 746–753.
197. Luo Y, Lode A, Wu C, *et al.*, 2015, Alginate/nanohydroxyapatite scaffolds with designed core/shell structures fabricated by 3D plotting and *in situ* mineralization for bone tissue engineering. *Acs Appl Mater Interfaces*, 7(12): 6541–6549.
198. Rifai A, Tran N, Dwm L, *et al.*, 2018, Polycrystalline diamond coating of additively manufactured titanium for biomedical applications. *Acs Appl Mater Interfaces*, 10(10): 8474–8484.
199. Chen H, Wang C, Xiao Y, *et al.*, 2016, Construction of surface HA/TiO 2 coating on porous titanium scaffolds and its preliminary biological evaluation. *Mater Sci Eng C Mater Biol Appl*, 70(Pt 2): 1047.
200. Chai Y C, Kerckhofs G, Roberts S J, *et al.*, 2012, Ectopic bone formation by 3D porous calcium phosphate–Ti6Al4V hybrids produced by perfusion electrodeposition. *Biomaterials*, 33(16): 4044–4058.
201. Liao H T, Lee M Y, Tsai W W, *et al.*, 2013, Osteogenesis of adipose-derived stem cells on polycaprolactone–β-tricalcium phosphate scaffold fabricated via selective laser sintering and surface coating with collagen Type I. *J Tissue Eng Regen Med*, 10(10): E337.
202. Chen C H, Lee M Y, Shyu V B, *et al.*, 2014, Surface modification of polycaprolactone scaffolds fabricated via selective laser sintering for cartilage tissue engineering. *Mater Sci Eng C*, 40: 389–397.
203. Huang W, Zhang H, Huang Y, *et al.*, 2011, Hierarchical porous carbon obtained from animal bone and evaluation in electric double–layer capacitors. *Carbon*, 49(3): 838–843.
204. Amin Y S, Van d S J, Chai Y C, *et al.*, 2014, Bone regeneration performance of surface–treated porous titanium. *Biomaterials*, 35(24): 6172–6181.
205. Cheng A, Humayun A, Cohen D J, *et al.*, 2014, Additively manufactured 3D porous Ti–6Al–4V constructs mimic trabecular bone structure and regulate osteoblast proliferation, differentiation and local factor production in a porosity and surface roughness dependent manner. *Biofabrication*, 6(4):

45007.

206. Shuai C, Yang Y, Feng P*, et al.*, 2018, A multi–scale porous scaffold fabricated by a combined additive manufacturing and chemical etching process. *Int J Bioprint,* 4(3): 133.
207. Ramier J, Boubaker M B, Guerrouache M*, et al.*, 2014, Novel routes to epoxy functionalization of PHA-based electrospun scaffolds as ways to improve cell adhesion. *J Polym Sci Part A Polym Chem*, 52(6): 816–824.
208. Wang X, Li Y, Hodgson P D*, et al.*, 2010, Biomimetic modification of porous TiNbZr alloy scaffold for bone tissue engineering. *Tissue Eng Part A*, 16(1): 309–316.
209. Hanson A D, Wall M E, Pourdeyhimi B*, et al.*, 2007, Effects of oxygen plasma treatment on adipose–derived human mesenchymal stem cell adherence to poly (L–lactic acid) scaffolds. *J Biomater Sci Polym Ed*, 18(11): 1387–1400.
210. Roh H S, Lee C M, Hwang Y H*, et al.*, 2016, Addition of MgO nanoparticles and plasma surface treatment of three–dimensional printed polycaprolactone/hydroxyapatite scaffolds for improving bone regeneration. *Mater Sci Eng C.*, 74: 1-608.
211. Roh H S, Jung S C, Kook M S*, et al.*, 2016, *In vitro* study of 3D PLGA/n–HAp/β–TCP composite scaffolds with etched oxygen plasma surface modification in bone tissue engineering. *Appl Surf Sci*, 388: 321–330.
212. Jeon H, Lee H, Kim G, 2014, A surface–modified poly(ε–caprolactone) scaffold comprising variable nanosized surface–roughness using a plasma treatment. *Tissue Eng Part C Methods*, 20(12): 951.
213. Jayanth N, Senthil P, Prakash C, 2018, Effect of chemical treatment on tensile strength and surface roughness of 3D–printed ABS using the FDM process. *Virtual Phys Prototyp,* 2018: 1–9.
214. Calignano F, 2018, Investigation of the accuracy and roughness in the laser powder bed fusion process. *Virtual Phys Prototyp*, 1: 1–8.